

# **Modeling of Current-voltage Characteristics of thin film Solar cells**

Md Shahnawaz Anjan

A Thesis

In the Department

of

Electrical and Computer Engineering

Presented in Partial Fulfillment of the Requirements

for the Degree of Master of Applied Science at

Concordia University

Montréal Québec Canada

May 2011

@ Md. Shahnawaz Anjan, 2011

**CONCORDIA UNIVERSITY  
SCHOOL OF GRADUATE STUDIES**

This is to certify that the thesis prepared

By: Md. Shahnawaz Anjan

Entitled: “Modeling of Current-voltage Characteristics of Thin Film Solar Cells”

and submitted in partial fulfillment of the requirements for the degree of

**Master of Applied Science**

Complies with the regulations of this University and meets the accepted standards with respect to originality and quality.

Signed by the final examining committee:

_____	Chair
Dr. D. Qiu	
_____	Examiner, External To the Program
Dr. A. Youssef (CIISE)	
_____	Examiner
Dr. X. Zhang	
_____	Supervisor
Dr. M. Z. Kabir	

Approved by: \_\_\_\_\_  
Dr. W. E. Lynch, Chair  
Department of Electrical and Computer Engineering

\_\_\_\_\_  
20\_\_\_\_\_

\_\_\_\_\_  
Dr. Robin A. L. Drew  
Dean, Faculty of Engineering and  
Computer Science

# ABSTRACT

## Modeling of Current-voltage Characteristics of thin film Solar cells

Md Shahnawaz Anjan

Energy crisis and environmental issue lead us to investigate renewable and green energy sources. Abundant source of green energy is sun light, which can be harvested in many different procedures. Solar panel is proved the most effective method for extracting energy from sun light. The second-generation thin film solar cells are increasingly promising for their cheaper production and better efficiency. Cells based on (i) polycrystalline CdTe, (ii) polycrystalline CuInGaSe<sub>2</sub> (CIGS) and (iii) hydrogenated amorphous Si (a-Si:H) absorbers are the three most potential photoconductors for thin film solar cells because of their excellent efficiency.

A realistic first principle analytical (preferably) model is essential for properly understanding the operating principles of a solar cell and optimizing its overall efficiency. Until now, few models were proposed in the literature but those models are either oversimplified or having too many fitting parameters. In this thesis we have proposed an analytical model to study the current-voltage characteristics of *pin/nip* structured cell especially CdS/CdTe thin film solar cells by incorporating exponential photon absorption, carrier trapping and carrier drift in the CdTe layer. An analytical expression for the external voltage dependent photocurrent is derived by solving the continuity equation for both electrons and holes. The overall load current is calculated considering the actual solar spectrum. The recombination current in the depletion

region dominates over the ideal diode current in CdTe solar cells. The solar cell efficiency depends critically on the transport properties of the carriers that drift towards the back contact. The photon absorption capability over a wide spectrum and good carrier transport properties of the absorber layer are equally important for achieving higher efficiency. The analytical model shows a very good agreement with the published experimental data on various thin film solar cells. The fitting of the model with the published experimental data considering the actual solar spectrum determines the carrier transport properties (mobility-lifetimes), the amount of reflection and scattering losses in various solar cells.

## ***ACKNOWLEDGMENTS***

Foremost, I would like to thank my wife Rehana Anjum Kakoli for her inspiration, support to complete the master's degree and especially for her patience during this endeavor. I am indebted to Dr. M. Zahangir Kabir for his continuous guidance, encouragement, help and financial support during the course of this research work. I also would like to extend my deepest gratitude to my parents, brother and sister for giving me encouragement, support throughout my life. This work would not be possible without the warm, healthy and knowledgeable discussion with all the members of our research group. I am grateful to my colleagues Mr. Md. Wasiur Rahman, Mr. Mazharul Huq Chowdhury, Mr. Md. Abdul Mannan and especially to Mr. Shaikh Asif Mahmood for their useful discussions. I also would like to show my gratitude to the professors and staffs at Concordia University. Finally, I am gratefully to our creator almighty ALLAH.

*To my loving  
parents & wife.*

# Table of Contents

List of Figures.....	ix
List of Tables.....	xi
List of Abbreviations .....	xii
<b>Chapter 1</b> Introduction.....	1
1.1 Energy Crisis in near future.....	1
1.2 Photovoltaic.....	2
1.3 Viability of Photovoltaic .....	3
1.4 The photovoltaic market .....	4
1.5 History of Solar Cell .....	5
1.6 Research Motivations .....	10
1.7 Research Objective .....	14
1.8 Thesis Outline .....	14
<b>Chapter 2</b> Background Theory .....	15
2.1 Solar radiation.....	15
2.2 Solar Cell material properties.....	17
2.2.1 Hydrogenated amorphous silicon (a-Si:H).....	17
2.2.2 Polycrystalline cadmium telluride (CdTe).....	19
2.2.3 Polycrystalline $\text{CuIn}_{1-x}\text{Ga}_x\text{Se}_2$ (CIGS) .....	22
2.3 Solar Cell Structures .....	22
2.3.1 Hydrogenated amorphous silicon (a-Si:H) cell structure .....	24
2.3.2 CdTe solar cell structure .....	26
2.3.3 CIGS solar cell structure .....	27
2.4 Existing Models for $J/V$ Characteristics of Thin film Solar Cells .....	28
2.5 Limitations of previous models .....	31
2.6 Summary .....	32
<b>Chapter 3</b> Modeling of Photocurrent .....	33
3.1 Introduction .....	33
3.2 Analytical Model .....	34
3.2.1 Continuity Equation of the System .....	35

3.2.2 Steady-state carrier concentration .....	36
3.2.3 Photocurrent .....	37
3.2.4 Forward Diode Current .....	40
3.2.5 Validity of neglecting of diffusion term in continuity equation .....	40
3.2.6 Photovoltaic cell Efficiency.....	41
3.3 Summary .....	42
<b>Chapter 4 Results And Discussions .....</b>	<b>43</b>
4.1 Introduction .....	43
4.2 CdTe solar cells .....	43
4.2.1 Effect of CdS window layer on <i>J-V</i> characteristics.....	48
4.2.2 Degradation of transport properties of the CdTe and CdS layers .....	50
4.3 CIGS solar cells .....	51
4.4 Amorphous Si solar cells .....	53
4.5 Summary .....	54
<b>Chapter 5 Conclusion, Contributions And Future Work .....</b>	<b>56</b>
5.1 Conclusion .....	56
5.2 Contributions .....	57
5.3 Suggestions for Future Work .....	58
<b>References .....</b>	<b>59</b>

# List of Figures

<b>Figure 1.1</b>	Fuel Consumption in 2009 .....	<b>2</b>
<b>Figure 1.2</b>	Cumulative World Installed PV Capacity (GW).....	<b>5</b>
<b>Figure 1.3</b>	The first generation of solar cells.....	<b>7</b>
<b>Figure 1.4</b>	$J/V$ curve of solar cell.....	<b>8</b>
<b>Figure 1.5</b>	$J/V$ curves for an a-Si $p-i-n$ solar cell: light, dark, and dark shifted downwards by $J_{sc}$ . The difference between the light and shifted curve is attributed to voltage dependent current collection losses in the light .....	<b>12</b>
<b>Figure 2.1</b>	Solar spectrum as a function of photon energy for AM1.5 .....	<b>16</b>
<b>Figure 2.2</b>	Atomic structure for (a) a crystalline semiconductor and (b) an amorphous semiconductor .....	<b>19</b>
<b>Figure 2.3</b>	a) The grain structure of polycrystalline solids. (b) The grain boundaries have impurity atoms, voids, misplaced atoms, and broken and strained bonds [22]....	<b>20</b>
<b>Figure 2.4</b>	Operation principle of basic p/n junction solar cell .....	<b>23</b>
<b>Figure 2.5</b>	Operation principle of heterojunction solar cell .....	<b>24</b>
<b>Figure 2.6</b>	Band diagram of the pin solar cell .....	<b>25</b>
<b>Figure 2.7</b>	Structure of CdTe Solar cell .....	<b>26</b>
<b>Figure 2.8</b>	Structure of CIGS Solar cell .....	<b>28</b>
<b>Figure 4.1</b>	Absorption coefficients of CdTe and CdS .....	<b>44</b>
<b>Figure 4.2</b>	Net current density versus voltage at three sun intensities. The symbols represent experimental data and the solid lines represent the theoretical fit to the experimental data. The experimental data were extracted from Ref. [15] ...	<b>45</b>
<b>Figure 4.3</b>	Theoretical net current density versus voltage for various levels of $\mu\tau'$ products of holes and electrons in CdTe Solar cells .....	<b>47</b>
<b>Figure 4.4</b>	Current-voltage characteristics of a CdTe solar cell as a function CdTe layer thickness .....	<b>48</b>
<b>Figure 4.5</b>	The effect of CdS layer thickness on the incident sun spectra at the CdTe layer. The sun spectra up to 1400 nm is shown since the solar cell is transparent to the photons of wavelengths that are higher than 900 nm .....	<b>49</b>
<b>Figure 4.6</b>	Efficiency vs. thickness of CdS layer graph .....	<b>50</b>

<b>Figure 4.7</b>	Current-voltage characteristics of a CdTe solar cell before and after stress. The symbols represent experimental data and the solid lines represent the theoretical fit to the experimental data. The experimental data were extracted from Ref [16] .....	<b>51</b>
<b>Figure 4.8</b>	Absorption coefficients of CIGS and a-Si .....	<b>52</b>
<b>Figure 4.9</b>	Current-voltage characteristics of a CIGS solar cell. The symbols represent experimental data and the solid lines represent the theoretical fit to the experimental data. The experimental data were extracted from Ref[25] .....	<b>53</b>
<b>Figure 4.10</b>	Current-voltage characteristics of an a-Si:H solar cell. The symbols represent experimental data and the solid lines represent the theoretical fit to the experimental data. The experimental data were extracted from Ref [44].....	<b>54</b>

## List of Tables

<b>Table 4.1</b> – CdS/CdTe Solar cell efficiency as a function of carrier range.....	<b>46</b>
---	-----------

## List of Abbreviations

PV	-	Photo Voltaic
Cd	-	Cadmium
Pb	-	Lead
Se	-	Selenium
a-Si	-	amorphous silicon
FF	-	Fill Factor
CdTe	-	Cadmium Telluride
CdS	-	Cadmium Sulfide
Cu <sub>2</sub> S	-	Copper Sulfide
CuInSe <sub>2</sub>	-	Copper Indium Selenide
CIGS	-	Copper Indium Gallium Selenide
AM	-	Air Mass
CIS	-	Copper Indium Selenide
ZnTe	-	Zink Telluride
ITO	-	Indium Tin Oxide
I <sub>0</sub>	-	Incident Photon flux
Cu(InGa)Se <sub>2</sub>	-	Copper Indium Gallium Selenide

# CHAPTER 1 INTRODUCTION

## 1.1 Energy Crisis in near future

The availability of economic and sustainable energy sources is vital for the subsistence of the human race. In 2008, 88.16% of the world's total energy consumption was supplied by burning oil, natural gas and coal (Figure 1.1) [1]. Power generated by the fossil fuel causes an emission of 31578 million ton of CO<sub>2</sub> in 2008 which is 1.6% higher than the previous year. These huge amounts of greenhouse gas increase the earth's average temperature. Scientists have confirmed, with a high degree of certainty, that the recent trend in global average temperatures is not a normal phenomenon [2]. Since climate modification is not possible, human beings must be careful in their use of energy sources and reduce the share of fossil fuels as much as possible by replacing their role with clean and environmentally friendly energy sources that are renewable, such as solar, wind, water, and biomass.

This, however, is an enormous challenge because we used approximately 452 quadrillion Btu ("Quads") of energy in 2008 and according to some estimates we will need double that amount to 900 Quads by 2040. Annual consumption of 900 Quads would correspond to an average power of 30 Terawatts ("TW"). If we decided to supply half of this energy, 15 TW, through nuclear power, we would have to build one average size (1000 MW) nuclear power plant everyday for the next 41 years. Estimates of the energy potential of other renewable sources such as wind, ethanol, hydroelectric, and geothermal lead to the same conclusion: humans consume an enormous amount of energy

compared to that can be obtained from any one of the renewable sources with the exception of direct sunlight. The sun can supply the amount of energy we used in all of the year 2008 in less than one hour. In fact, covering approximately a 130,000 square mile (e.g., 360 miles  $\times$  360 miles) section (4% of the Sahara desert) with 15% efficient solar cells and 50% packing would provide 15 TW. [3] These data lead us to a conclusion that solar energy will be the prime source of energy in the near future.

### Consumption by Fuel

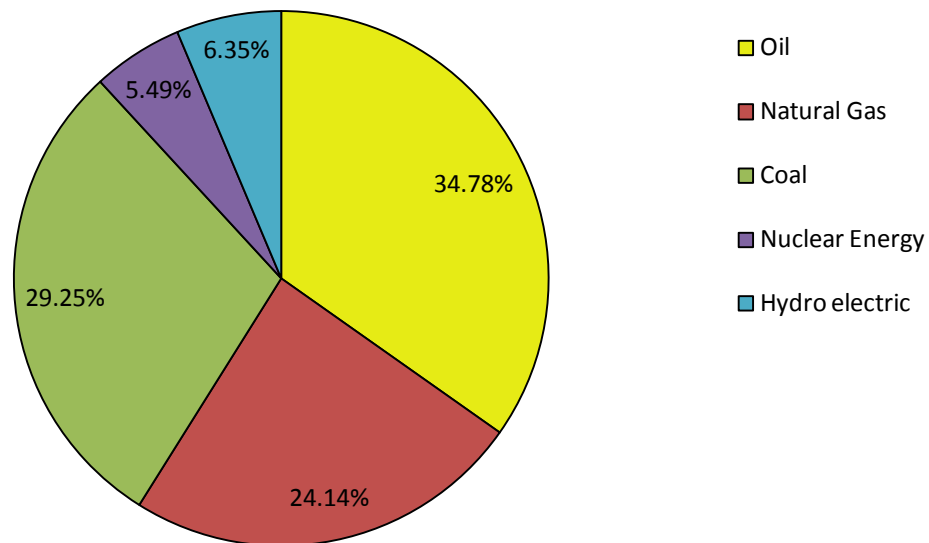


Figure 1.1 Fuel Consumption in 2009 [1]

### 1.2 Photovoltaic

Solar photovoltaic energy conversion is a single step process, which converts available light into electrical energy. According to quantum theory, light is made up of packets of energy named photons whose energy depends only on the frequency of light.

The energy of photons in sunlight is sufficient to excite electrons from lower energy level to higher energy level in semiconductor materials. In this process, pairs of electron and holes are created. In photovoltaic devices, there is some built-in asymmetry, which pulls the photo generated electron and holes in the opposite sides and a potential difference is created. A current will flow in the external circuit if the two sides are connected by an external load.

### **1.3 Viability of Photovoltaic**

In order to be a fully sustainable energy technology, photovoltaic has to qualify in certain indicators of viability such as:

1. The energy pay-back time,
2. The CO<sub>2</sub> emissions and
3. The end-of-life management and recycling.

The energy payback time of the photovoltaic systems depends not only on the energy content of the entire photovoltaic system, but also on the local irradiation conditions. An energy pay-back time of 2.5-3 years has been estimated for present-day grid connected roof-top installations in Southern Europe conditions. This should be compared to the expected life times of over 30 years of the present PV systems.

Quite opposite to the fossil energy sources, the CO<sub>2</sub> emissions associated with photovoltaic energy conversion occur almost entirely during system manufacturing instead of system operation. Therefore the CO<sub>2</sub> emissions depend on the CO<sub>2</sub> emission

factor of the local energy utility system, which provides the energy for the manufacture of the PV system. The requirement of sustainability of photovoltaic energy conversion extends beyond the operating lifetime of a PV system.

Depending on the PV technology the cells contain small amounts of different hazardous and regulated materials, such as Cd, Pb and Se, which raises concerns about their disposal into municipal landfills. However, the technology for recycling the solar cells already exists and it can be considered also economically feasible.

#### **1.4 The photovoltaic market**

After the development of the first silicon solar cell in 1954, the solar cells were used primarily in space applications until about the mid-70s [4]. Since then the solar cells have found applications in customer electronics, small scale remote residential power systems, as well as in communication and signaling. However, it is only in the second half of last decade that grid connected photovoltaic (PV) systems entered the market with significant contribution as a result of the intensive roof programs in Japan, Germany and US. Today's photovoltaic market has exceeded 6.43 gigawatt per year [5] and represents growth of 6% over the previous year. The PV industry generated \$38 billion in global revenues in 2009 and world solar cell production reached a consolidated figure of 9.34 GW in 2009, (Figure-1.2) with thin film production accounting for 18% of that total.

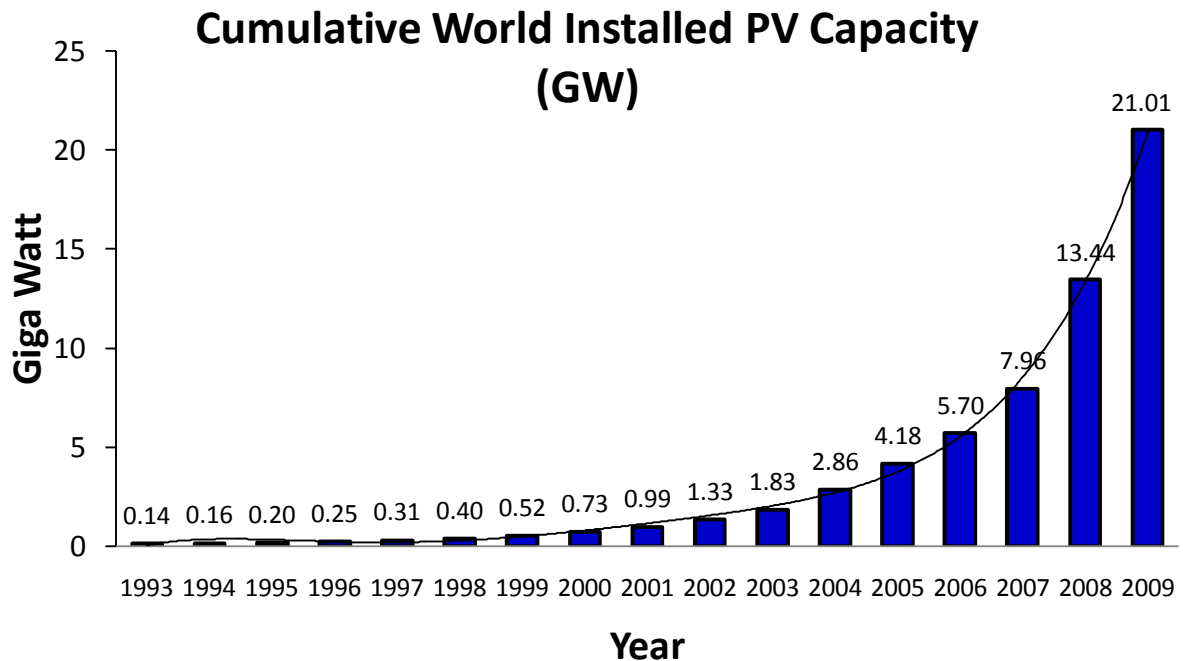


**Figure 1.2** Cumulative World Installed PV Capacity (GW) [6]

## 1.5 History of Solar Cell

The development of the solar cell stems from the work of the French physicist Edmund Becquerel in 1839. Becquerel discovered the photovoltaic effect while experimenting with silver coated platinum electrode in an electrolyte solution; he observed that voltage developed when light fell upon the electrode. In 1876 William Adams and Richard Day saw that a photocurrent would flow in a sample of selenium when contacted by two heated platinum contacts. A rectifying junction had been formed between the semiconductor and the metal contact in this early photovoltaic device. About 20 years later in 1894, Charles Fritts constructed the first true solar cells using junctions formed by coating the semiconductor selenium with an ultrathin, nearly transparent layer

of gold. Fritts's devices were very inefficient, transforming less than 1 percent of the absorbed light into electrical energy.

By 1927 another metal semiconductor-junction solar cell, in this case made of copper and the semiconductor copper oxide, had been demonstrated. By the 1930s both the selenium cell and the copper oxide cell were being employed in light-sensitive devices, such as photometers, for use in photography. These early solar cells, however, still had energy-conversion efficiencies of less than 1 percent. This impasse was finally overcome with the development of the silicon solar cell by Russell Ohl in 1941. In 1954, three other American researchers, G.L. Pearson, Daryl Chapin, and Calvin Fuller, demonstrated a silicon solar cell capable of 6-percent energy-conversion efficiency when used in direct sunlight. This efficiency is six times higher than the previous but at an estimated production cost of some \$200 per watt. So these cells were not considered for power generation for several decades.

The oil-dependent western world faces the crisis in energy supply in 1970s which led to a growth interest in alternative source of energy. Photovoltaic was a subject of intense interest during this period. In that period lots of studies were performed for the development of device structure, material and efficiency. Seeking of lower production cost led to alternative materials such as polycrystalline silicon, amorphous silicon, other thin film materials and organic materials. From the efficiency point of view research trend led to tandem and multiple band gap design.

The first generation of solar cells is simple p/n junction cell (Figure 1.3). These solar cells are manufactured from extremely pure silicon. A typical diagram of the cell is given bellow.

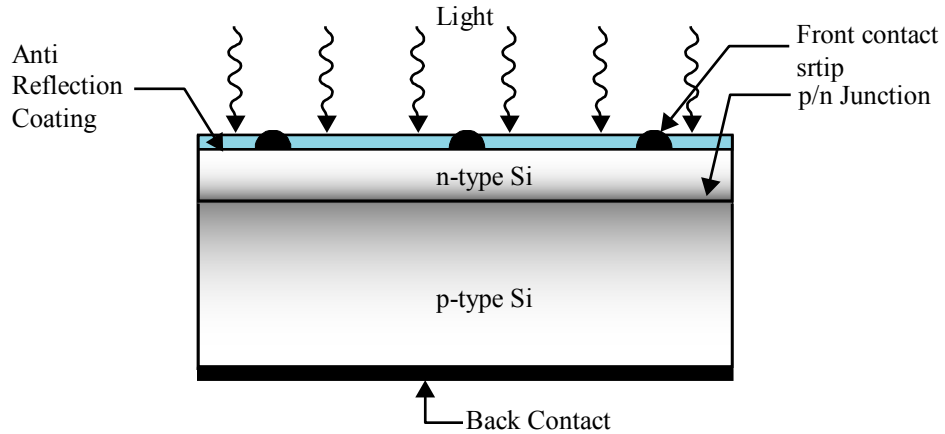


**Figure 1.3** The first generation of solar cells

The main advantage of first generation solar cells is its efficiency which is approaching their theoretical maximum efficiency of 33%. The **efficiency** of the solar cell is defined as the ratio of power produced by the cell to the solar power incident on the cell.

$$\eta = \frac{J_m V_m}{P_{in}} \quad (1)$$

Where  $P_{in}$  is the incident solar power,  $J_m$  and  $V_m$  are defined as the corresponding current and voltage of the intersection of the maximum power line of the  $J$ - $V$  curve of solar cell. Figure 1.4 illustrates the  $J$ - $V$  curve of solar cell,  $J_m$  and  $V_m$ ,  $J_{sc}$  and  $V_{sc}$ . The **Fill factor**(FF) can be defined as

$$FF = \frac{J_m V_m}{I_{sc} V_{oc}} \quad (2)$$

The FF will be unity if the  $J$ - $V$  curve is essentially rectangular, which is one of the most desirable feature. Combining equations (1) and (2), we get

$$\eta = \frac{FF \times J_{sc} V_{oc}}{P_{in}} \quad (3)$$

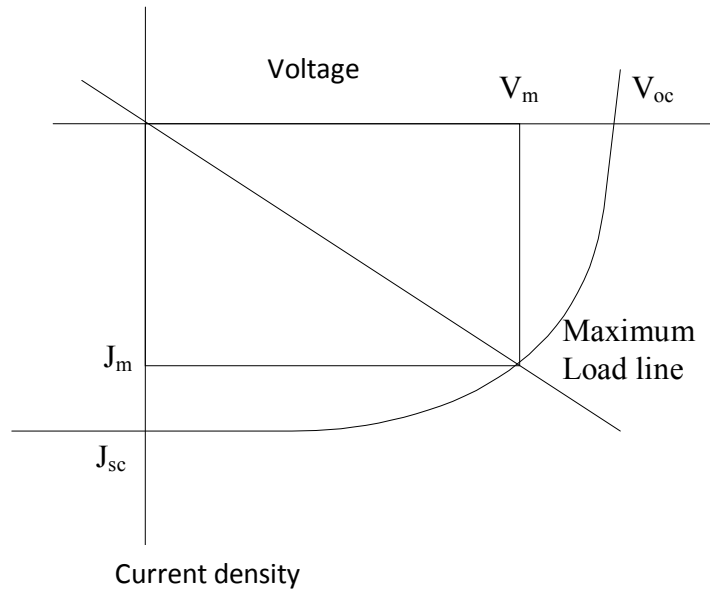


**Figure 1.4** Current-voltage ( $J$ - $V$ ) characteristics curve of a solar cell

The main disadvantage of the first generation solar cell is its production cost, as it needs very high quality silicon. It is not thought that first generation cells will be able to provide energy more cost economic than the fossil fuel sources.

The second-generation solar cell, which has been under intense development for the 90s and early 2000s, are low-cost thin-film solar cells. These cells use minimal

materials and cheap manufacturing processes. Cells based on (i) polycrystalline CdTe, (ii) polycrystalline  $\text{CuIn}_{1-x}\text{Ga}_x\text{Se}_2$  (CIGS) and (iii) hydrogenated amorphous Si (a-Si:H) absorbers are the three most potential photoconductors for thin film solar cells because of their excellent efficiency [7]. The subscript  $x$  represents the mole fraction. These thin materials are usually produced by physical or chemical deposition techniques, which can be applied to large areas and fast throughout. The term “thin film” refers more to the solar cell technologies with mass-production possibilities rather than the film thickness. The main advantage of thin-film solar cells is low cost due to low cost of processing and materials.

Both the CdTe and CIGS based cells are  $p$ - $n$  heterojunction cells, where a very thin layer ( $\sim 0.1 \mu\text{m}$ ) of CdS acts as a highly doped  $n$ -layer and CdTe or CIGS layer acts as lightly doped  $p$ -type absorber layer. The thickness of the  $p$ -layer is few micrometers. The incident photons are mainly absorbed in the  $p$ -layer and the photo carriers are collected by the built-in electric field in this layer. The a-Si:H solar cells use  $p$ - $i$ - $n$  type structure where the  $p$  and  $n$ -layers are few nm and the  $i$ -layer is  $\sim 1 \mu\text{m}$  thick. The incident photons are mainly absorbed in the  $i$ -layer in a-Si:H solar cells. Polycrystalline and amorphous semiconductors contain intrinsic defects, which increase the density of traps and recombination centers, and reduce diffusion lengths. Therefore, an extended built-in electric field in low-doped absorber layer is used to aid carrier collection. The voltage dependent charge collection in the depleted absorber layer is the dominant charge collection mechanisms in thin film solar cells.

Third generation solar cells are just a research target, and do not really exist yet. The goals of third generation solar cell research are low-cost, high efficiency cells. The

goals are thin-film cells that use novel approaches to obtain efficiencies in the range of 30-60%. Some analysts predict that third generation cells could start to be commercialized sometime around 2020, but this is just a guess. Technologies associated with third generation solar cells include multijunction photovoltaic cells, tandem cells, nanostructured cells to better pick up incident light, and using excess thermal generation to enhance voltages or carrier collection.

## 1.6 Research Motivations

Solar cell efficiency refers to the fraction of incident light energy converted to electrical energy. Sun's spectrum, semiconductor material properties and the device structure control the efficiency. For a given solar spectrum, the efficiency depends on the following four main factors.

1. **Light absorption:** Some photons are not absorbed for photon energy,  $h\nu < \text{Bandgap energy, } E_g$ . Here  $h$  is the Planck constant and  $\nu$  is the frequency of light. Again, high-energy photons are absorbed near the surface and are mostly lost by recombination. This effect can reduce efficiency to 40-50%. Choosing appropriate material that can absorb the whole sun spectrum reduces the light absorption loss.
2. **Reflection of photons from the surface:** A fraction of incident photons can be reflected from the top surface. Without antireflection coating in Si, the reflection loss can be 35%.
3. **Charge collection efficiency:** All photo generated carriers must be collected. There should not be trapping or recombination of carriers. The collection efficiency is typically 95 % in crystalline Si solar cells.

4. **Nonideal factors:** The photo generated carrier has to travel a surface semiconductor region to reach the nearest finger electrode. This rough carrier path introduces an effective series resistance,  $R_s$ . Again, a fraction of carriers can flow through the edges of the devices internally instead of flowing through the external load. This effect can be represented by an effective internal shunt or parallel resistance,  $R_p$ . Series and shunt resistances typically reduce the efficiency to 90%.

An antireflection coating can minimize the reflection loss. To minimize the effects of factors 1, 3 and 4, we need to choose appropriate materials and design (e.g., optimum thicknesses of different layers in solar cells). Therefore, accurate modeling of current-voltage characteristics is necessary in order to optimize the material and design for achieving peak efficiency. Efficient solar cell performance requires minimizing the forward diode current  $J_F(V)$  and maximizing the light generated current  $J_L$ . The latter process requires maximizing both the optical generation in the absorber layer and the collection of the photo-generated carriers. High purity crystalline Si is used in first generation solar cells and, therefore, the charge collection efficiency is almost 95 %. Moreover, the operational principles of crystalline Si solar cells are well understood and the analytical model for  $J$ - $V$  characteristics is found in standard textbook [8].

Polycrystalline and amorphous semiconductors contain intrinsic defects, which increase the density of traps and recombination centers, and reduce diffusion lengths. Therefore, an extended built-in electric field in low-doped absorber layer is used to aid carrier collection. The voltage dependent charge collection in the depleted absorber layer is the dominant charge collection mechanisms in thin film solar cells. Collection losses

can be especially significant in some thin-film solar cells due to their high absorption and short diffusion lengths. Voltage dependent photocurrent collection, or  $J_L(V)$ , losses have been observed in all thin-film solar cells:  $\text{Cu}_2\text{S}$  [9],  $\text{CdTe}$ [10],[11],[12],  $\text{CuInSe}_2$  based solar cells [13],[14],[15], and a-Si based solar cells[16]. The behavior of voltage dependent photocurrent is shown in Figure 1.5 [17].

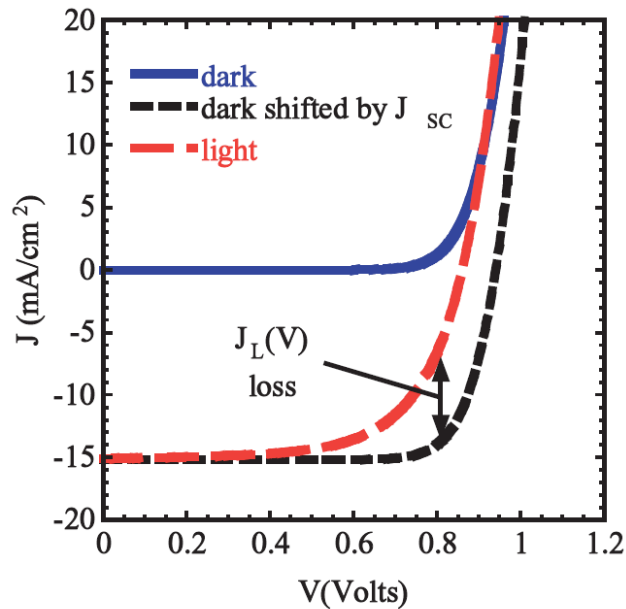


**Figure 1.5**  $J$ - $V$  curves for a  $\text{CdTe}$  solar cell: light, dark, and dark shifted downwards by  $J_{SC}$ . The difference between the light and shifted curve is attributed to voltage dependent current collection losses.

The principle of superposition, commonly assumed in analysis of solar cells, requires that the light curve should be the same as the dark curve, only shifted downwards by a constant photocurrent, that is,  $J_{SC}$ . Superposition generally occurs in crystalline Si solar cells. A steady decrease in current over the range of flat region of dark current is sometimes explained as the effect of shunt resistance. However, a true shunt

would affect dark current the same way as the light current. Clearly, the light curve does not follow the principle of superposition in CdTe solar cells. The difference between the light and shifted curve is attributed to voltage dependent current collection losses. Therefore, we need to formulate the  $J$ - $V$  curve from the first principles of charge collection mechanism. Until now, few models were proposed in the literature but all those models have severe limitations.

The textbook of Wagemann and Eschrich [18] gives a closed-form expression for the dark  $J/V$  equation, but this expression holds only for voltages around the point  $V = 0$ . Hegeduset *al.* reviewed a few theoretical models to describe the current-voltage ( $J$ - $V$ ) characteristics in thin film solar cells [17]. They have shown that the most successful model calculates the photocurrent by considering carrier drift and utilizing Hecht collection efficiency formula in the nearly intrinsic absorber layer [17]. However, the previous model has made an unrealistic assumption that all the carriers are generated at the top interface of the absorber layer for all incident photons. The previous model has also used a number of fitting parameters such as maximum photocurrent with complete charge collection, reverse saturation current, effective attenuation coefficient for the whole solar spectrum. Therefore, a realistic first principle analytical (preferably) model is necessary with minimum number of fitting parameters.

## 1.7 Research Objective

In general, the objectives of this thesis are:

- (a) To develop an analytical model based on first principle charge carrier transport mechanisms to study the current-voltage characteristics of thin film solar cells by incorporating full sun spectrum, exponential photon absorption, carrier trapping and carrier drift in the CdTe layer.
- (b) To analyze the effects of various factors that controls the  $J/V$  characteristics.
- (c) To verify the model with the published experimental data on CdTe, CIGS and a-Si:H solar cells.

## 1.8 Thesis Outline

This thesis consists of five chapters. Following this introductory chapter, few basic theories and important terminologies are discussed in chapter two. The proposed model and the first principle formulation of analytical expression for the photocurrent are described in chapter three. Results and discussions of the model calculations are presented in chapter four. Conclusion, Contributions and suggested future work are presented in chapter five.

## CHAPTER 2 BACKGROUND THEORY

The built in asymmetry in the solar cell is the driving force to generate current by separating electron and hole generated by photon absorption by the device. This phenomenon is known as photo-voltaic or photo-electric effect. The photoelectric effect is the basic physical process by which a PV cell converts sunlight into electricity. When light shines on a PV cell, it may be reflected, absorbed, or pass right through. But only the absorbed light generates electricity. The energy of the absorbed light is transferred to electrons in the atoms of the PV cell. With their new found energy, these electrons escape from their normal positions in the atoms of the semiconductor PV material and become part of the electrical flow, or current, in an electrical circuit by means of built in electric field or carrier concentration gradient. In this chapter we give a brief description about the operation of some well-established solar cell devices.

### 2.1 Solar radiation

In every second  $6 \times 10^{11}$  kg of hydrogen ( $H_2$ ) converted to helium in sun by nuclear fusion reaction with a net mass loss of about  $4 \times 10^3$  kg. This amount of mass is converted into energy as the form of electromagnetic radiation following the Einstein relation  $E=mc^2$  and the amount is nearly  $4 \times 10^{20}$  joules. The total mass of sun is about  $2 \times 10^{30}$  kg and this amount of energy is available for 10 billion year from this mass [19].

Water vapor attenuates the power in infrared region and ozone layer absorbs power in the ultraviolet region of the sun spectrum. The degree to which atmosphere affect the sun

light received at the earth surface is define by the “air mass”. The secant of the angle between the sun and the zenith is called the air mass. Air mass 1.5 condition (sun at 45° above the horizon) represent a satisfactory energy-weighted average for terrestrial application. The intensity of sunlight per nm wavelength range per  $cm^2/sec$  for AM1.5 as a function of wavelength is shown in Figure 2.1 [20]. To convert the wavelength to photon energy we have used the relationship [19],

$$\lambda = \frac{c}{\nu} = \frac{1.24}{hv(eV)} \mu m \quad (4)$$

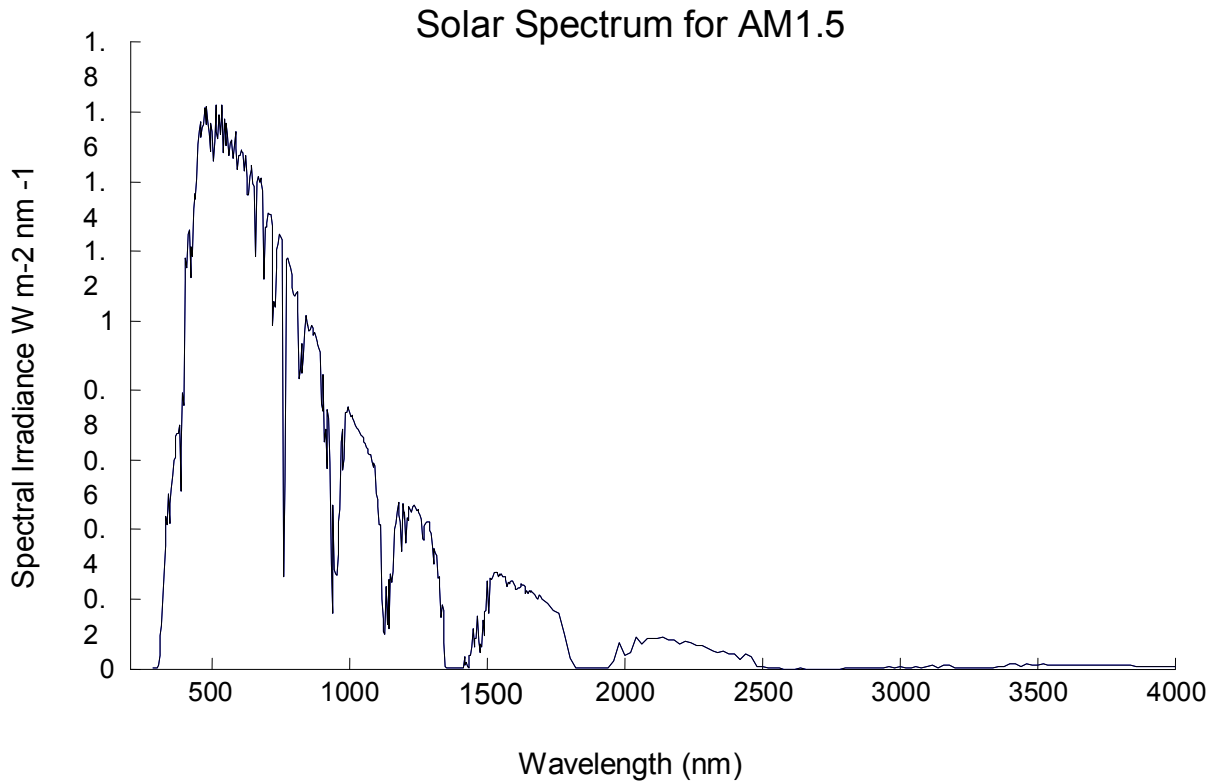


**Figure 2.1** Solar spectrum as a function of photon energy for AM1.5.

## **2.2 Solar Cell material properties**

### **2.2.1 Hydrogenated amorphous silicon (a-Si:H)**

Amorphous materials lack periodicity in their atomic structure which is the characteristic property of crystals. Due to the absence of lattice periodicity, the physical and electrical properties of amorphous materials are different from their crystalline state. The density of state variation in amorphous structure controls the basic electrical properties which can be determined experimentally. Due to the absence of lattice periodicity in the amorphous phase the basic Bloch theorem of solid-state physics can no longer be applied and, consequently, that no meaningful reciprocal space can be defined for amorphous materials. Thus, standard solid-state-physics theories become useless. However, the physical properties of amorphous materials are necessarily not very different from those of their crystalline analogues. Over short distances the atomic arrangements in amorphous compounds are very similar to crystalline phase. All material properties that are mainly determined by short-range interactions will, therefore, also be similar. This includes mechanical and vibrational properties, magnetic properties, or electronic band structures. But the properties that result from long-range order, such as mobility, will be strongly affected. The interesting aspect is, the disorder in the atomic lattice gives rise to physical phenomena that are absent in the corresponding crystal. Localization of electronic wave functions, the possibility of mono-atomic defects, and the appearance of extra low-energy vibrational excitations are such instances.

The crystalline structure is characterized by a highly ordered arrangement of atoms as depicted in Figure 2.2 (a). Each atom in the network has the same coordination

number, and the bond lengths and bond angles between the atoms are identical. Throughout the crystal this high degree order exists. If we ignore the surface states, the equilibrium position of each atom in the network is precisely known from any other position in the network. This type of order is described as long-range order.

In an amorphous semiconductor, slight variations exist in the bond length and bond angle between the atoms in the network which are sufficient to destroy the spatial periodicity of the network. The disorder in the network introduces localized electronic states; states where the electron wave function is localized to a particular position in the semiconductor. The energy location and density of these localized states have a profound impact on the electronic and optical properties of amorphous semiconductors. The atomic structure of amorphous semiconductors contains defects that affect its properties. In the amorphous structure, the only specific structural feature of the atoms is the coordination number of an atom. The elementary defect of an amorphous semiconductor is a coordination defect when an atom has too many or too few bonds. In Figure 2.2(b) an under-coordinated and an over-coordinated defect are shown as U and O respectively. These defects introduce additional localized electronic states in the electronic structure of the amorphous material. Unoccupied bonds commonly called as dangling bonds are very dominant structural defect in amorphous silicon (a-Si). The hydrogen binds to dangling bond defects and removes the corresponding electronic states in the band gap, thus eliminating most of the trapping and recombination centers. The 5-10 atomic percent of hydrogen is bonded to the silicon atoms, mostly in the form of Si:H bonds, either isolated or on the surface of small voids.

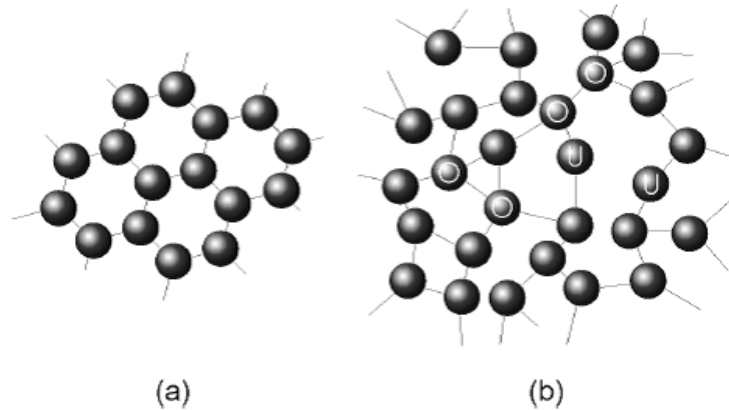


**Figure 2.2** Atomic structure for (a) a crystalline semiconductor and (b) an amorphous semiconductor.

The key advance in the development of a-Si:H alloys for solar cells was the discovery that the band gap can be changed by varying the incorporation of hydrogen[21], carbon or germanium. Alloying a-Si with carbon or germanium create additional defect states, relatively good optoelectronic properties can be obtained over band gaps ranging from  $\sim 1.3$  eV ( $\sim 75$  at. %Ge) to  $\sim 2.1$  eV ( $\sim 15$  at. %C). This ability to tune the band gap of a-Si based alloys has been an underlying factor in the improvement in the performance of a-Si based solar cells which has led to initial efficiencies as high as 13% in laboratory [22]. The effective electron and hole mobilities are,  $\mu_e = 0.25$ - $1$   $\text{cm}^2/\text{Vs}$  and  $\mu_h = .003$   $\text{cm}^2/\text{Vs}$  and the nominal bandgap is  $E_g = 1.75$  eV.

### 2.2.2 Polycrystalline cadmium telluride (CdTe)

*Polycrystalline* material is not a single crystal as a whole, but composed of many small crystals randomly oriented in different directions. The small crystals in polycrystalline solids are called grain. These grains have irregular shapes and

orientations as shown in Figure 2.3. A polycrystalline material has grain boundaries where differently oriented crystals meet. The atoms at the grain boundaries obviously cannot follow their normal bonding tendency because the crystal orientation suddenly changes across the boundary. Therefore, there are voids, and stretched and broken bonds at the grain boundary. In addition, there are misplaced atoms in grain boundary, which cannot follow the crystalline pattern on either side of the boundary. In many polycrystalline materials, impurities tend to segregate in the grain boundary region. The atomic arrangement in the grain boundary region is considered as *disorder*.

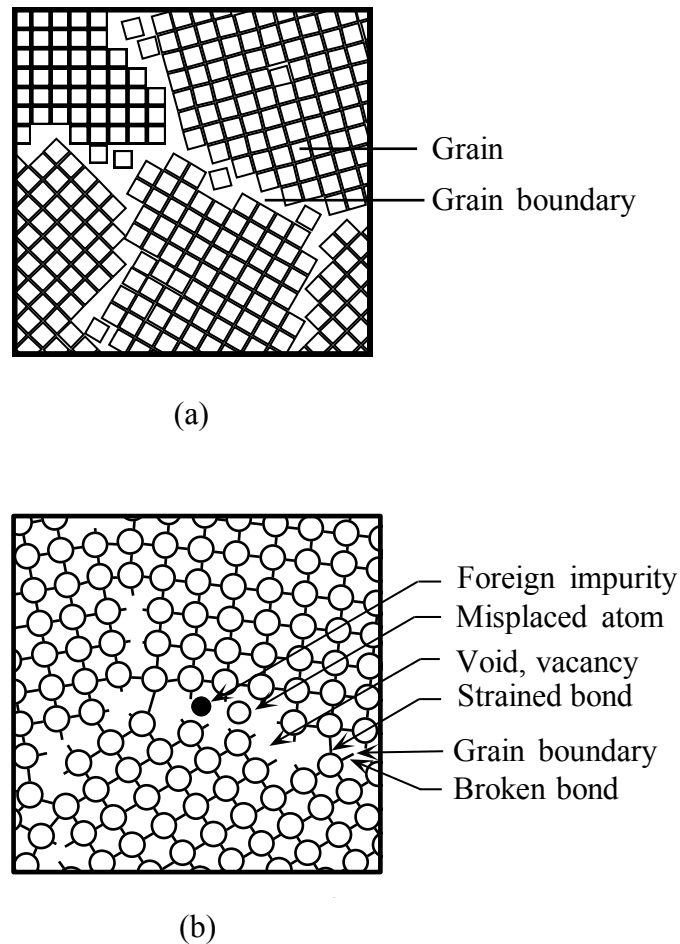


**Figure 2.3** (a) The grain structure of polycrystalline solids. (b) The grain boundaries have impurity atoms, voids, misplaced atoms, and broken and strained bonds [23].

Polycrystalline CdTe is very well suited for use as active material in thin-film solar cells. It has an energy gap of 1.45 eV, and therefore is well adapted to the spectrum of solar radiation. The energy gap of CdTe is 'direct', leading to very strong light absorption. Its electron affinity is 4.2-4.5 eV with effective density of states  $7.9 \times 10^{17} \text{cm}^{-3}$  in conduction band and  $1.3 \times 10^{19} \text{cm}^{-3}$  in valence band. The relative dielectric constant  $\epsilon_r$  is 10.36. Because of the high optical absorption coefficient (higher than a-Si, much higher than crystalline silicon), a few micrometers of CdTe is sufficient to absorb all the incident sunlight. As a result a minority carrier diffusion length of the order of one  $\mu\text{m}$  is sufficient to allow all the generated carriers to be collected at the contacts: this greatly relaxes the materials quality requirements.

The CdTe has wurtzite crystal structure, like GaAs. It suffers from a high density of native defects such as excess Te atoms at the grain boundaries, which give rise to defect states deep in the band gap. Cadmium telluride is the only stable Cd-Te compound in the Cd-Te phase diagram, and it melts congruently, this property makes easier deposition of CdTe. But being a binary compound the occurrence of native defects makes the precise doping difficult which is also true for ternary and quaternary compounds such as  $\text{Cu}(\text{In,Ga})\text{Se}_2$  and for amorphous materials. CdTe has a strong tendency to grow as an essentially highly stoichiometric p-type semiconductor film and can form an p-n heterojunction with CdS (CdS has a rather wide energy gap of 2.4 eV and grows highly doped n-type material under usual film deposition techniques). The CdTe is p-type to make good ohmic contact to the CdTe/metal. However, higher doping reduces the minority carrier lifetime. Therefore, the doping in CdTe is limited to  $(1-2) \times 10^{14} \text{cm}^{-3}$ .

### 2.2.3 Polycrystalline $\text{CuIn}_{1-x}\text{Ga}_x\text{Se}_2$ (CIGS)

Copper indium diselenide ( $\text{CuInSe}_2$ , or CIS) is direct gap semiconductor with a bandgap of around 1eV. Addition of Ga improves the photovoltaic characteristics by raising the band gap as well as the electronic properties of the rear contact. The nominal bandgap of CIGS (with  $x = 0.3$ ) is 1.2 eV, which is suitable for absorbing the solar spectra. The compound forms the chalcopyrite crystal structure. The carrier lifetime is in the range of few nanosecond.

## 2.3 Solar Cell Structures

The actual structural design of a photovoltaic device depends on the properties of the material used in the PV cell. Both homojunction and heterojunction structures are used solar cells.

**Homojunction solar cell** - In its simplest form, the solar cell consists of a junction formed between  $n$ -type and  $p$ -type semiconductors of the same material. Crystalline silicon is the primary example of this kind of cell. When a photon, with energy greater than the band gap of the semiconductor, passes through the solar cell, it may be absorbed by the material. This absorption takes the form of a band-to-band electronic transition, so an electron/hole pair is generated. If the generation occurs in the depletion region they are separated by the electric field causing one quantum of charge to flow through an external load. This is the origin of the solar cell's photocurrent, and is shown in Figure 2.4.

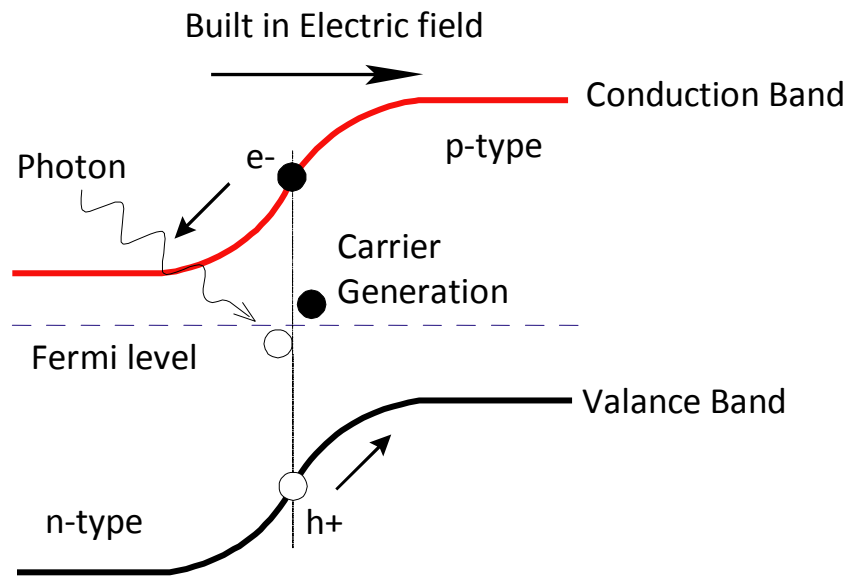


**Figure 2.4** Operation principle of basic *p/n* junction solar cell

**Heterojunction Device** - An example of this type of device structure is a CIS cell, where the junction is formed by contacting two different semiconductors - CdS and CuInSe<sub>2</sub>. This structure is often chosen for producing cells made of thin-film materials that absorb light much better than homojunction. Heterojunction devices have an inherent advantage over homojunction devices, which require materials that can be doped both *p*- and *n*-type. Many PV materials can be doped either *p*-type or *n*-type, but not both. Again, because heterojunctions don't have this constraint, many promising PV materials can be investigated to produce optimal cells. Also, a high band gap window layer reduces the cell's series resistance. The window material can be made highly conductive, and the thickness can be increased without reducing the transmittance of light. As a result, light-

generated electrons can easily flow laterally in the window layer to reach an electrical contact. The band structure of heterojunction is shown in figure 2.5.

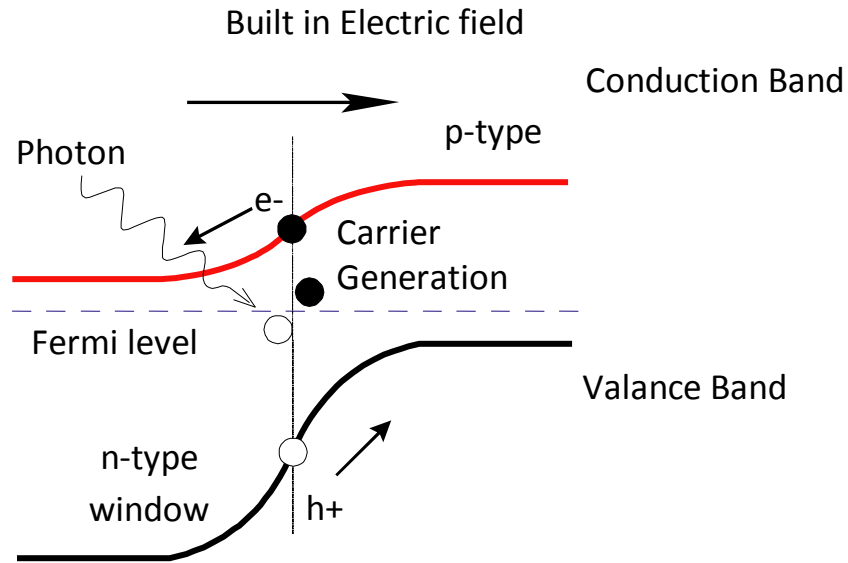


**Figure 2.5** Operation principle of heterojunction solar cell

### 2.3.1 Hydrogenated amorphous silicon (a-Si:H) cell structure

Typically, amorphous silicon thin-film cells use a *p-i-n* structure. The basic scenario is as follows: A three-layer sandwich is created, with a middle intrinsic layer between an *n*-type layer and a *p*-type layer. This geometry sets up an electric field between the *p*- and *n*-type regions that stretches across the middle intrinsic region. Light generates free electrons and holes in the intrinsic region, which are then separated by the electric field.

In the  $p-i-n$  amorphous silicon (a-Si) cell, the top layer is  $p$ -type a-Si, the middle layer is intrinsic silicon, and the bottom layer is  $n$ -type a-Si. Amorphous silicon has many atomic-level electrical defects when it is highly conductive. So very little current would flow if an a-Si cell had to depend on diffusion. However, in a  $p-i-n$  cell, current flows because the free electrons and holes are generated within the influence of an electric field, rather than having to move toward the field. Figure 2.6 shows the band diagram of the  $p-i-n$  diode/solar cell. The electric field in the  $i$ -layer is practically uniform.

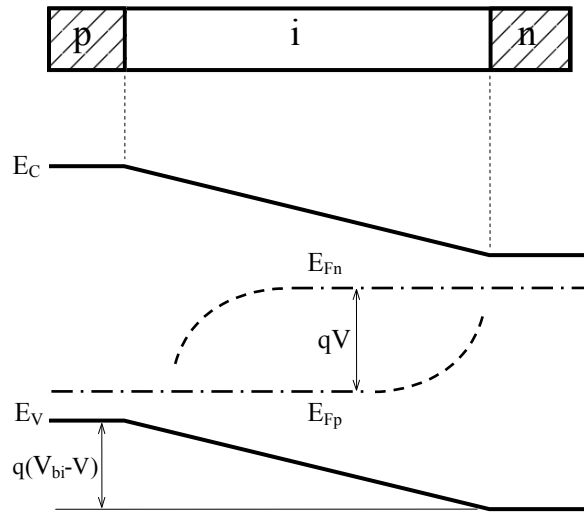


**Figure 2.6** Band diagram of the  $p-i-n$  solar cell.  $V_{bi}$  is built-in potential and  $V$  is the external voltage.

In thermal equilibrium, the electron (minority carrier) concentration  $n_{po}$  in the  $p$ -type layer, and the hole concentration  $p_{no}$  in the  $n$ -type layer, are given by  $p_{no} = n_i^2/N_p$  and  $n_{po} = n_i^2/N_n$ , where  $n_i$  is the intrinsic concentration of the given semiconductor and  $N_n$  and  $N_p$  are the doping density of the  $n$  and  $p$ -layers respectively.[24]

### 2.3.2 CdTe solar cell structure

The CdTe based solar cells have a superstrate device structure of glass/SnO<sub>2</sub>/CdS /CdTe/metal [25, 26] as shown in Figure 2.7. The CdTe based cells are *p-n* heterojunction cells, where a very thin layer (~0.1 μm) of CdS acts as a highly doped *n*-layer and CdTe acts as lightly doped *p*-type absorber layer. The thickness of the *p*-layer is few micrometers. The incident photons are mainly absorbed in the *p*-layer and the photo carriers are collected by the built-in electric field in this layer.

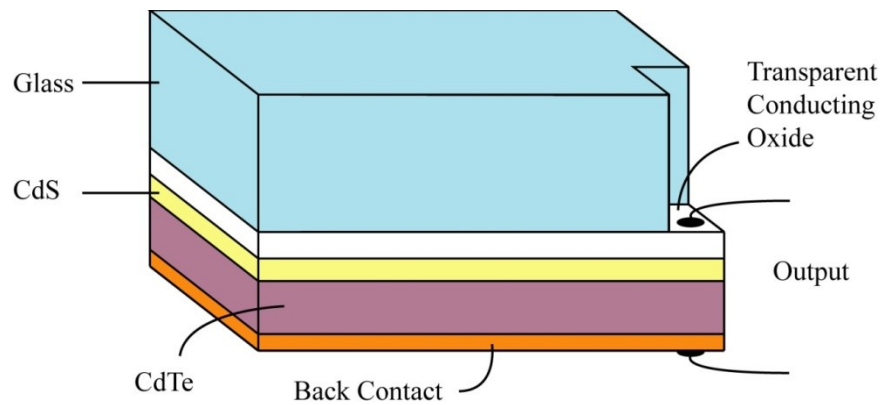


**Figure 2.7** Structure of CdTe Solar cell

The solar cell is produced on a substrate of ordinary window glass, because it is transparent, strong and cheap. The glass is typically 2-4 mm thick, and it protects the active layers from the environment and provides the entire device's mechanical strength. The outer face of the plane often has an anti-reflective coating to enhance its optical properties. The transparent conducting oxide is usually made of tin oxide or indium tin oxide (ITO) and it acts as the front contact to the device. It is needed to reduce the series resistance of the device, which would otherwise arise from the thinness of the CdS layer.

The polycrystalline Cadmium sulfide (CdS) layer is *n*-type doped. Being a wide band gap material ( $E_g \sim 2.4$  eV at 300K) it is transparent down to wavelengths of around 515 nm, and so is referred to as the window layer. Below that wavelength, some of the light will still pass through to the CdTe, due the thinness of the CdS layer ( $\sim 100$  nm). The Cadmium telluride (CdTe) layer is polycrystalline *p*-type doped. Its energy gap (1.42 eV) is ideally suited to the solar spectrum, and it has a high absorption coefficient for energies above this value. It acts as an efficient absorber and is used as the *p* side of the junction. Because it is less highly doped than the CdS, the depletion region is mostly within the CdTe layer. The CdTe absorber layer is fully depleted and the built-in electric field  $F$  is nearly uniform across the absorber layer because of its lightly doping. This is therefore the active region of the solar cell, where most of both the carrier generation and collection occur. The thickness of this layer is typically around 1-5  $\mu\text{m}$ . The back contact is usually gold or aluminum and it should provide a low resistance ohmic connection to the CdTe layer. Due to its high conductivity, the metal layer needs only be a few tens of nanometers in thickness.

### **2.3.3 CIGS solar cell structure**

The CIGS based solar cells have a substrate device structure of grid/ZnO/CdS /CIGS/Mo/glass [25,26] as shown in Figure 2.8. The CIGS based cells are *p-n* heterojunction cells, where a very thin layer ( $\sim 0.1$   $\mu\text{m}$ ) of CdS acts as a highly doped *n*-layer and the polycrystalline CIGS layer acts as lightly doped *p*-type absorber layer. The thickness of the *p*-layer is few micrometers. The incident photons are mainly absorbed in the *p*-layer and the photo carriers are collected by the built-in electric field in this layer.

The CIGS absorber layer is fully depleted and the built-in electric field  $F$  is nearly uniform across the absorber layer because of its lightly doping. CIGS cells are always prepared on a molybdenum coated glass substrate, as Mo is needed to make an Ohmic contact.

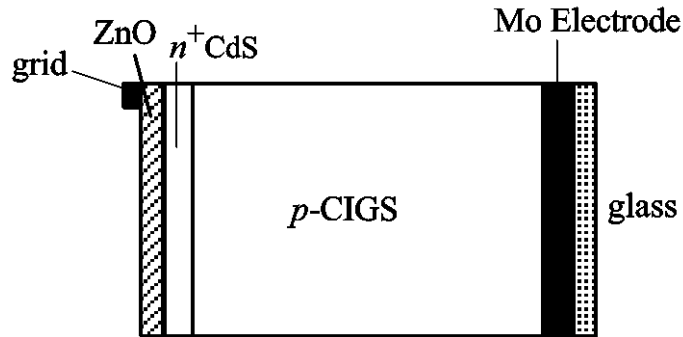


**Figure 2.8** Structure of CIGS Solar cell

## 2.4 Existing Models for $J/V$ Characteristics of Thin film Solar Cells

All the previous models for describing the  $J/V$  characteristics of thin film solar cell are based on the concept that the total photo generated current  $J_L(V)$  can be expressed as a product of a constant current density  $J_{LO}$  and a voltage dependent charge collection efficiency  $\eta_c(V)$  [16] [17] [27]. That is,

$$J_L(V) = J_{LO} \times \eta_c(V) \quad (5)$$

where  $J_{LO}$  is the maximum photocurrent with complete collection. It is assumed that  $J_{LO}$  is the photo current obtained at sufficiently large reverse bias and linearly dependent on light intensity but not on the voltage.  $\eta_c(V)$  is the voltage dependent collection efficiency

and varies from 1 at reverse bias to 0 at some forward bias  $V_O$ . The net current density from a solar cell is

$$J(V) = J_d(V) - J_L(V) \quad (6)$$

where  $J_d(V)$  is the forward diode current. It can be extracted from the above equation that the deviation of  $J/V$  curve from elevated diode current is completely dependent on charge collection efficiency  $\eta_c(V)$ . There exists three expressions for  $\eta_c(V)$ . These are given below.

**Model-1:** Considering interface recombination, drift collection losses and the interface collection factor (ICF), the first model for voltage dependent charge collection efficiency was developed [9][10][13] and expressed as[17]

$$\eta_c(V) = \frac{\mu F_0(V)}{S + \mu F_0(V)} \quad (7)$$

Here  $\mu$  is the minority carrier mobility,  $F_0(V)$  is the field at the interface, and  $S$  is the interface recombination velocity. Assuming a  $p-n$  heterojunction field at the interface can be written as

$$F_0(V) = \left[ \frac{2qN_A}{\varepsilon} (V_{bi} - V) \right]^{1/2} \quad (8)$$

Here  $N_A$  is the doping concentration of the absorber layer. The drawback of this model is that it has four fitting parameter namely  $\mu$ ,  $S$ ,  $N_A$  and  $V_{bi}$ , which are not readily known.

**Model-2:** The second model uses simplified  $p$ - $n$  junction or heterojunction structure to describes the collection in a conventional way by incorporating voltage dependent depletion width  $W(V)$  and a diffusion length  $L$  [13].

$$\eta_c(V) = 1 - \frac{\exp\{-\Delta^{-1}\}}{1 + \alpha(\lambda)L} \quad (9)$$

Where  $\Delta = 1/\alpha(\lambda)W(V)$  and  $\alpha(\lambda)$  is the wavelength-dependent absorption coefficient and  $L$  is the diffusion length. Voltage dependent depletion width  $W(V)$  is the primary dominating factor in the expression of collection efficiency which can be shown as

$$W(V) = \left[ \frac{2\varepsilon}{qN_A} (V_{bi} - V) \right]^{1/2} \quad (10)$$

Similar to the first model it has also four fitting parameter namely  $\alpha(\lambda)$ ,  $L$ , acceptor carrier density  $N_A$  and  $V_{bi}$  (built in potential), some of them are hard to determine for CdTe or for a given CdTe device. This model leads to a single value of  $\alpha$  to represent the effective or weighted CdTe absorption coefficient.

It is assumed in equation (9) that minority carriers generated within the depletion region  $W(V)$  or those which diffuse to the edge of the depletion region are collected without any losses due to their rapid transit time crossing the high field space charge region. That means within the high field region, collection efficiency is 100% for any carrier, which is equivalent to saying that the recombination lifetime ( $\tau_R$ ) in the space charge region greatly exceeds the drift time ( $\tau_D$ ) across it [17]. This is the general phenomenon for  $p/n$  junction crystalline solar cell structure but not a valid assumption in thin film solar cells.

**Model-3:** The third model for  $\eta_c(V)$  is based on the losses due to recombination of carrier within high field depletion region  $W$ . A detailed study measures the probability of drifting of carrier that passes without being lost due to recombination through the high field depletion region and the result of that study shows that losses in a high field region are given by  $1-\exp(-\tau_R/\tau_D)$ . The drift time across the region  $W$  is  $\tau_D=W^2/\mu V$  if field is assumed uniform. It was developed to analyze voltage dependent collection in a-Si *p-i-n* solar cells [28] according to the Hecht-like equation for the limiting carrier [29]

$$\eta_c(V) = X(V) \left[ 1 - \exp(-X(V)^{-1}) \right] \quad (11)$$

Where

$$X(V) = X_c \left( 1 - V/V_0 \right) \quad (12)$$

## 2.5 Limitations of previous models

Hegedus et al. reviewed a few theoretical models to describe the current-voltage (*J-V*) characteristics in thin film solar cells [17]. They have shown that the most successful model calculates the photocurrent by considering carrier drift and utilizing Hecht collection efficiency formula (model 3 above) in the nearly intrinsic absorber layer [17]. However, the previous model has made an unrealistic assumption that all the carriers are generated at the top interface of the absorber layer for all incident photons. The previous model has also used a number of fitting parameters such as maximum photocurrent with complete charge collection, reverse saturation current, effective

attenuation coefficient, series resistance and carrier ranges. Therefore, a first principle model with physically achievable fitting parameters is necessary.

## **2.6 Summary**

Necessary theoretical concepts regarding the modeling of *pin/nip* solar cell have been briefly discussed in this chapter. These concepts will be very helpful to understand our model. We also discuss some existing models in brief in this chapter. In our next chapter, we are going to discuss our proposed model for the  $J/V$  characteristics of thin film solar cells.

# CHAPTER 3 MODELING OF PHOTOCURRENT

## 3.1 Introduction

There has been an active theoretical and experimental research to improve the performance of thin film solar cells. Hegeduset *al.* reviewed a few theoretical models to describe the current-voltage ( $J$ - $V$ ) characteristics in thin film solar cells [17]. They have shown that the most successful model calculates the photocurrent by considering carrier drift and utilizing Hecht collection efficiency formula (model 3 of section 2.4) in the nearly intrinsic absorber layer [17]. However, the previous model has made an unrealistic assumption that all the carriers are generated at the top interface of the absorber layer for all incident photons. The previous model has also used a number of fitting parameters such as maximum photocurrent with complete charge collection, reverse saturation current, effective attenuation coefficient, series resistance and carrier ranges. The incident photons are absorbed exponentially across the absorber layer. In this thesis, we solve the continuity equation for both electrons and holes considering exponential photon absorption, exponential electron-hole pair generation across the absorber layer, carrier trapping and carrier drift in the absorber layer. We obtain an analytical expression for the external voltage  $V$  dependent photocurrent assuming the electric field remains uniform in the absorber layer. The overall load current is calculated considering the effect of voltage dependent forward dark current and the actual solar spectrum.

The present model only uses carrier ranges and series resistance as fitting parameters and thus eliminates other fitting parameters such as reverse saturation current

and effective attenuation coefficient. We analyze the  $J$ - $V$  characteristics and efficiency in CdTe solar cells with varying carrier transport properties and operating conditions. The model is verified with the published experimental data on all three types of solar cells mentioned above. The fitting of the model with the published experimental data considering the actual solar spectrum determines the carrier transport properties (mobility-lifetimes), the amount of reflection and scattering losses in various solar cells.

### 3.2 Analytical Model

The photon absorption in the highly doped top  $p$  or  $n$  layers will contribute a negligible current because of their very short diffusion length and very thin width. The photo generated electrons and holes are drifted in opposite directions by the built-in electric field in the absorber layer (e.g., the  $p$ -layer in CdTe or CIGS and  $i$ -layer in a-Si:H solar cells). Electrons drift towards the radiation-receiving contact (top contact) and holes drift towards the bottom contact in CdTe or CIGS solar cells. Unlike CdTe solar cells, holes drift towards the radiation receiving contact (top contact) and electrons drift towards the bottom contact in a-Si:H solar cells. The following assumptions are made to allow the problem to be analytically tractable [30];

(i) The thermal equilibrium concentration of charge carriers is negligibly small because of high bandgap materials,

(ii) The absorber layer is fully depleted and the built-in electric field  $F$  is nearly uniform across the light absorber layer because of its lightly doping,

(iii) The diffusion of carriers is negligible compared with their drift in the fully depleted absorber layer (explained later),

(iv) A constant drift mobility  $\mu$  and a single lifetime  $\tau'$  are assigned to each type of carriers (holes and electrons).

The voltage dependent electric field near the top interface of the absorber layer is slightly higher than that near the bottom interface, the photo generated carriers will drift with a slightly higher velocity near the top interface compared to that near the bottom interface. Therefore, assuming an average drift velocity of the carriers throughout the absorber layer will not make any significant difference in the calculation of charge collection.

### 3.2.1 Continuity Equation of the System

Considering the assumptions mentioned above, the steady-state continuity equation for the carriers that drift towards the bottom electrode is [30],

$$\frac{\partial c_b}{\partial t} = -\mu_b F \frac{\partial c_b}{\partial x} - \frac{c_b}{\tau'_b} + G e^{-\alpha x} = 0, \quad (13)$$

and the steady-state continuity equation for the carriers that drift towards the top electrode is,

$$\frac{\partial c_t}{\partial t} = \mu_t F \frac{\partial c_t}{\partial x} - \frac{c_t}{\tau'_t} + G e^{-\alpha x} = 0, \quad (14)$$

where  $\alpha(\lambda)$  is the absorption coefficient of the material,  $\lambda$  is the photon wavelength,  $x$  is the depth in the absorber layer from the top interface of this layer,  $G$  is the carrier generation rate at  $x = 0$ ,  $c_b$  is the photo generated carrier concentration for the charge carriers drifting towards the bottom contact and  $c_t$  is the photo generated carrier concentration for the charge carriers drifting towards the top contact.  $F$  represents the electric field in the absorber-layer. The subscript  $b$  and  $t$  refers to the carrier type drifting towards the bottom and top contact respectively. In CdTe and CIGS solar cells, the top layer is  $n$ -type, but in a-Si:H cells, the top layer is  $p$ -type. In  $pin$  structure,  $c_b$  represents electrons but in  $np$  it represents holes. The reason for this kind of notation is to make the model applicable for both kinds of orientation.

### 3.2.2 Steady-state carrier concentration

General solution of equation (13) with constant C1 is

$$c_b = \left( -\frac{\tau'_b G \exp\left(-\frac{x(\alpha\tau'_b\mu_b F - 1)}{\tau'_b\mu_b F}\right)}{\alpha\tau'_b\mu_b F - 1} + C1 \right) \exp\left(-\frac{x}{\tau'_b\mu_b F}\right)$$

And the solution of equation (14) with constant C2 is

$$c_t = \left( \frac{\tau'_t G \exp\left(-\frac{x(\alpha\tau'_t\mu_t F + 1)}{\tau'_t\mu_t F}\right)}{\alpha\tau'_t\mu_t F + 1} + C2 \right) \exp\left(\frac{x}{\tau'_t\mu_t F}\right)$$

In the above expressions value of  $C1$  and  $C2$  can be obtained by imposing proper boundary condition. As the carriers start drifting immediately after generation under the influence of field,  $c_b(x=0) = 0$  and  $c_t(x= W) = 0$ , where  $W$  is the width of the absorber layer.

Therefore, the steady-state carrier concentrations in the absorber layer are

$$c_b(x, \lambda) = \frac{G\tau'_b}{1 - \alpha\mu_b F\tau'_b} \left( e^{-\alpha x} - e^{\frac{-x}{\mu_b F\tau'_b}} \right). \quad (15)$$

and

$$c_t(x, \lambda) = \frac{G\tau'_t}{1 + \alpha\mu_t F\tau'_t} \left( e^{-\alpha x} - e^{\frac{x}{\mu_t F\tau'_t}} \right). \quad (16)$$

### 3.2.3 Photocurrent

The photocurrent density for the carriers drifting towards the bottom contact is, [30, 31 , 32],

$$\begin{aligned} j_b(\lambda, V) &= \frac{e\mu_b F}{W} \int_0^W c_b(x, \lambda) dx \\ &= \frac{eGW}{(\tau_b^{-1} - \Delta^{-1})} \left[ \Delta \left( 1 - e^{-\frac{1}{\Delta}} \right) - \tau_b \left( 1 - e^{-\frac{1}{\tau_b}} \right) \right], \end{aligned} \quad (17)$$

where  $e$  is the elementary charge,  $\Delta (=1/\alpha W)$  is the normalized absorption depth,  $\tau_b (= \mu_b \tau'_b F/W)$  is the normalized carrier lifetime (carrier lifetime per unit transit time) for

the carriers drifting towards the bottom contact. Since  $F$  is voltage dependent,  $\tau_b$  is also voltage dependent and so does  $j_b$ .

Similarly, the photocurrent density for the carriers drifting towards the top contact is,

$$j_t(\lambda, V) = \frac{eGW}{(\tau_t^{-1} + \Delta^{-1})} \left[ \Delta \left( 1 - e^{-\frac{\lambda}{\Delta}} \right) - \tau_t \left( e^{-\frac{\lambda}{\Delta}} - e^{-\frac{\lambda}{\Delta} - \frac{\lambda}{\tau_t}} \right) \right], \quad (18)$$

where  $\tau_t = \mu_t \tau'_t F/W$  and the subscript  $t$  refers to the carrier type drifting towards the top contact (e.g., the subscript  $t$  represents electrons in CdTe solar cells). The resultant photocurrent density,  $j_L(\lambda, V) = j_b(\lambda, V) + j_t(\lambda, V)$ . Therefore, the photocurrent density,

$$j_L(\lambda, V) = eGW \left\{ (\tau_b^{-1} - \Delta^{-1})^{-1} \left[ \Delta \left( 1 - e^{-\frac{\lambda}{\Delta}} \right) - \tau_b \left( 1 - e^{-\frac{\lambda}{\tau_b}} \right) \right] \right. \\ \left. + (\tau_t^{-1} + \Delta^{-1})^{-1} \left[ \Delta \left( 1 - e^{-\frac{\lambda}{\Delta}} \right) - \tau_t \left( e^{-\frac{\lambda}{\Delta}} - e^{-\frac{\lambda}{\Delta} - \frac{\lambda}{\tau_t}} \right) \right] \right\} \quad (19)$$

The electron-hole pair generation rate can be written as,

$$G(\lambda) = \alpha(\lambda) e^{-\alpha_1 d} [1 - R(\lambda)] \lambda I_0(\lambda) / hc, \quad (20)$$

where  $c$  is the speed of light,  $h$  is the Plank constant,  $I_0$  is the intensity of the solar spectra ( $W/cm^2 \cdot nm$ ),  $R$  is the total reflection and scattering loss factor,  $\alpha_1$  and  $d$  are the absorption coefficient and thickness of the thin top semiconductor layer (the  $n$ -layer in CdTe or GIGS, and  $p$ -layer in a-Si:H solar cells). The other losses include shading from the grid, absorption in the top  $SnO_2$  layer, and incomplete electron-hole pair (EHP) generation in the absorber layer [26].

The total photo generated current density is obtained by integrating over all incident photon wavelengths of the solar spectrum,

$$J_L(V) = \int_0^{\infty} j_L(\lambda, V) d\lambda \quad (21)$$

The net current density from a solar cell is

$$J(V) = J_d(V) - J_L(V) \quad (22)$$

where  $J_d(V)$  is the forward diode current. The external voltage dependent electric field is given by [26],

$$F(V) = \frac{V_0 - V_j}{W} = \frac{V_0 - (V - JR_s)}{W} \quad (23)$$

where  $R_s$  is the effective series resistance including all contact resistances,  $V_j (= V - JR_s)$  is the junction voltage, and  $V_0$  is the flat-band voltage so that  $J_L(V) = 0$  at  $(V - JR) = V_0$ . The flat-band voltage  $V_0$  is slightly higher (typically  $\sim 0.1$  V) than the open circuit voltage  $V_{OC}$ . It is expected that the electric field reduces to zero when the applied junction voltage is equal to the built-in potential  $V_{bi}$ . However, it is found that the electric field collapses to zero just beyond  $V_{OC}$  and little less than  $V_{bi}$  [26]. Therefore,  $V_0$  is considered as a fitting parameter.

### 3.2.4 Forward Diode Current

The forward diode current can be written as,

$$J_d(V) = J_0 \exp\left[\frac{e(V - JR_s)}{AkT}\right] \quad (24)$$

Where  $J_0$  is the reverse saturation current of the  $p/n$  junction,  $A$  is the diode ideality factor,  $k$  is the Boltzmann constant, and  $T$  is the absolute temperature. For  $p/n$  junction with small depletion region  $J_0$  can be expressed as [19]

$$J_0 = \frac{qD_p p_{no}}{L_p} + \frac{qD_n n_{po}}{L_n}$$

But if the depletion region is thick, recombination current within p-region should be dominant over ideal diffusion current [25]. Therefore, the reverse saturation current can be written as [33],

$$J_0 = \frac{en_i W}{\sqrt{\tau'_e \tau'_h}} \quad (25)$$

where  $n_i$  is the intrinsic carrier concentration of the absorber layer.

### 3.2.5 Validity of neglecting of diffusion term in continuity equation

If the injected carrier concentration decays exponentially, the carrier concentration can be written as

$$c(x) = Be^{-\alpha x}$$

where  $B$  is the carrier concentration at  $x = 0$ . The drift and diffusion current components are,

$$J_{drift} = e\mu Fc,$$

and  $J_{diff} = -eD \frac{dc}{dx}$ .

Taking,  $F \approx (V_{bi} - V)/W$  and using Einstein relation, the ratio of the diffusion current to the drift current is,

$$\left| \frac{J_{diff}}{J_{drift}} \right| = \frac{D\alpha}{\mu F} = \frac{D}{\mu \frac{(V_{bi} - V)}{\alpha L}} = \frac{D}{\mu \Delta (V_{bi} - V)} = \frac{V_t}{\Delta (V_{bi} - V)}$$

where  $V$  is the external voltage,  $L$  is the total photoconductor thickness and  $V_t = kT/e$  is the thermal voltage. Taking  $\Delta \sim 1$  and operating voltage,  $(V_{bi} - V) = 0.4$  V, the ratio of diffusion current to the drift current at room temperature is  $\sim 0.06$ . Therefore, the diffusion current component is negligible compared to its drift component in the depletion region.

### 3.2.6 Photovoltaic cell Efficiency

Equation (22) represents the current-voltage relationship for the device, which predicts the output power of the cell known as  $J$ - $V$  characteristic. On a  $J$ - $V$  plot, the vertical axis refers to current and the horizontal axis refers to voltage. The fill factor and efficiency can easily be determined from  $J$ - $V$  curve as described in section 1.5.

### **3.3 Summary**

In this chapter, we have discussed the proposed simplified model for calculating  $J$ - $V$  characteristics of thin film solar cells considering the actual solar spectrum. The present model only uses carrier ranges and series resistance as fitting parameters and thus eliminates other fitting parameters such as reverse saturation current and effective attenuation coefficient. The fitting of the model with the published experimental data considering the actual solar spectrum determines the carrier transport properties (mobility-lifetimes), the amount of reflection and scattering losses in various solar cells. In the next chapter, we will make theoretical analysis based on our proposed model and apply the model to various thin film solar cells. We will compare our results with the published experimental data.

# CHAPTER 4 RESULTS AND DISCUSSIONS

## 4.1 Introduction

In this chapter, we analyze the  $J$ - $V$  characteristics and efficiency in CdTe solar cells with varying carrier transport properties and operating conditions. The model is verified with the published experimental data on all three types of solar cells mentioned above. The  $J$ - $V$  characteristics of various solar cells are calculated by iteratively solving equations (19) – (25). The incident photon flux  $I_0(\lambda)$  is taken as the air mass (AM) 1.5 global spectrum from the ASTM G-173-03 standard [20]. We calculate the efficiency of various cells in different conditions. The theoretical model is applied to all three different thin film solar cells mentioned above.

## 4.2 CdTe solar cells

The theoretical model is verified by fitting with the published experimental data on CdTe solar cells. The absorption coefficients for CdTe and CdS are obtained from the absorption curves in Ref. [34]. Absorption coefficients of polycrystalline CdTe and CdS as a function of photon wavelength are shown in figure 4.1. The CdS layer significantly absorbs photons up to 500 nm of wavelength, and thus can reduce the photo current and its overall efficiency. The CdTe layer can effectively absorb photons up to 800 nm of wavelength, where the absorption coefficient is higher than  $2 \times 10^4 \text{ cm}^{-1}$  and the corresponding absorption depth is 0.5  $\mu\text{m}$ . Therefore, the CdTe layer thickness of 1.0  $\mu\text{m}$  can effectively absorb photons up to 800 nm of wavelength.

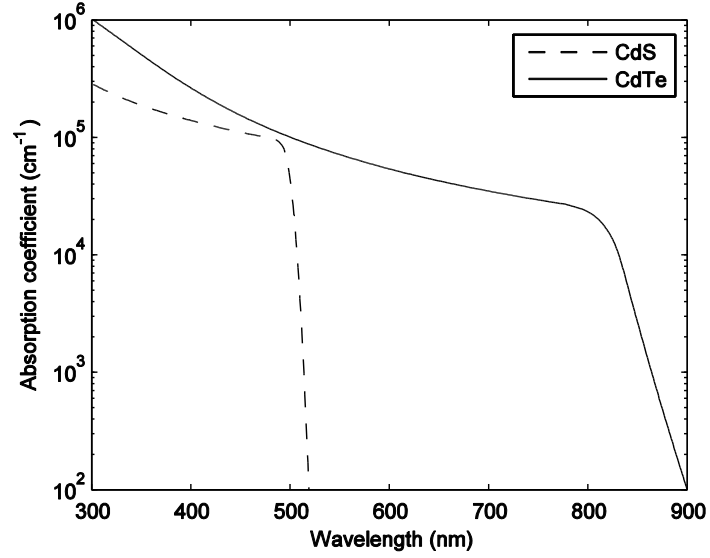


**Figure 4.1** Absorption coefficients of CdTe and CdS.

Figure 4.2 shows the  $J$ - $V$  curves of a CdS/CdTe solar cell at three sun intensities (100, 32, and 10 % of 1.5 AM global spectrum). The CdTe layer was deposited by vapor transport (VT) method. The symbols represent experimental data and the solid lines represent the theoretical fit to the experimental data. The experimental data were extracted from Fig. 6 of Ref [17]. The CdTe thickness is 1.8  $\mu\text{m}$ . The CdS thickness is assumed as 0.2  $\mu\text{m}$ . The theoretical model shows a very good agreement with the experimental data. The best fit  $\mu\tau'$  of holes and electrons are  $\mu_h\tau'_h = 10^{-6} \text{ cm}^2/\text{V}$  and  $\mu_e\tau'_e = 1.8 \times 10^{-5} \text{ cm}^2/\text{V}$ , which are consistent with the  $\mu\tau'$  values for CdTe [35, 36]. Assuming typical values for electrodeposited CdTe layer,  $\mu_h = 5 \text{ cm}^2/\text{V-s}$  [36] and  $\mu_e = 180 \text{ cm}^2/\text{V-s}$  [17] the carrier lifetimes become,  $\tau'_h = 0.2 \mu\text{s}$  and  $\tau'_e = \tau'_h = 0.1 \mu\text{s}$ . Note that a similar fitting was obtained by the previous model [17] using three additional fitting parameters (maximum photocurrent with complete charge collection, reverse saturation current, an

effective attenuation coefficient for the whole solar spectrum). Moreover, it also failed to distinguish the electron and hole transport properties and thus mentioned an effective mobility-lifetime product of  $8.4 \times 10^{-7} \text{ cm}^2/\text{V}$  by fitting the experimental data with the single carrier Hecht collection efficiency formula. The other fitted parameters in Fig 4.2 are:  $V_0 = 0.8 \text{ V}$ ,  $A = 1.8$ ,  $R_s = 6 \Omega\text{-cm}^2$ , and  $R = 0.25$ . The diode quality factor is 1.8, which implies that the recombination current dominates over the diffusion current.

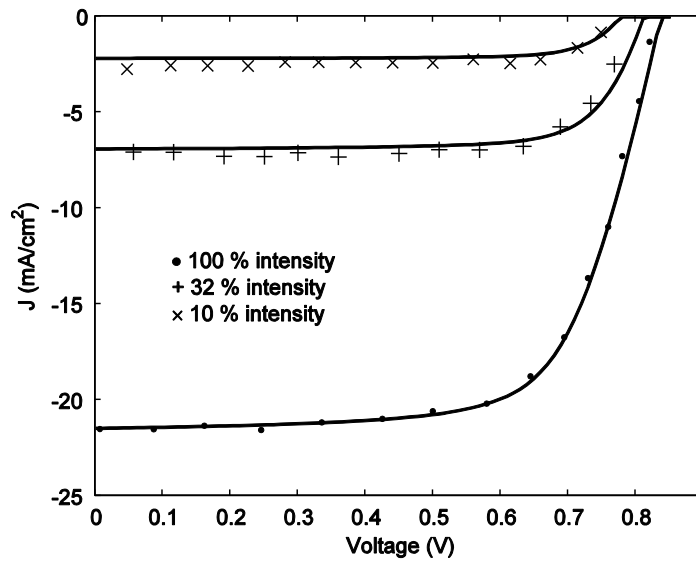


**Figure 4.2** Net current density versus voltage at three sun intensities. The symbols represent experimental data and the solid lines represent the theoretical fit to the experimental data. The experimental data were extracted from Ref. [17].

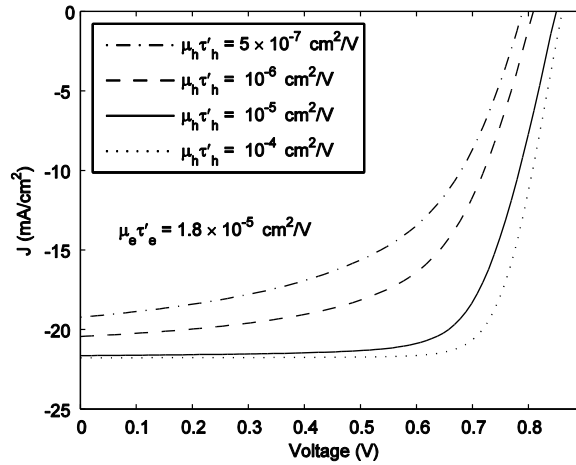
The EHPs are generated exponentially across the CdTe layer. Since the photon absorption coefficient up to 900 nm of wavelength is very high, the EHPs are mainly generated near the  $n$ - $p$  interface in the CdTe layer. Therefore, electrons quickly move towards the top electrode and holes have to move a much longer distance towards the bottom electrode. Thus, the charge collection should mainly be controlled by the hole

transport properties [37]. Figure 4.3 (a) and (b) show the  $J$ - $V$  characteristics of CdS/CdTe solar cells for various levels of  $\mu\tau'$  products of holes and electrons. All other parameters in Figure 4.3 are the same as in Figure 4.2. The theoretical overall efficiency varies from 8.2 % to 14.3 % by changing the  $\mu_h\tau'_h$  values from  $5\times 10^{-7}$   $\text{cm}^2/\text{V}$  to  $10^{-4}$   $\text{cm}^2/\text{V}$ , whereas it varies from 10.3 % to 12.4 % by changing the  $\mu_e\tau'_e$  values from  $10^{-7}$   $\text{cm}^2/\text{V}$  to  $10^{-4}$   $\text{cm}^2/\text{V}$ . The following table shows cell efficiency for various values of  $\mu_h\tau'_h$ .

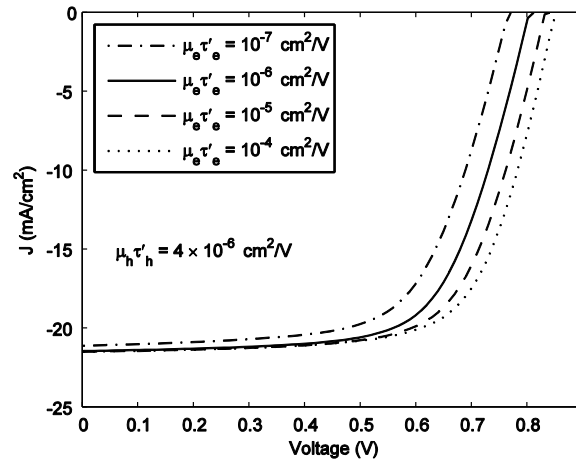
**Table 4.1** CdS/CdTeSolar cell efficiency as a function of carrier range.

$\mu_h\tau'_h$ ( $\text{cm}^2/\text{V}$ )	$1\times 10^{-7}$	$1\times 10^{-6}$	$1\times 10^{-5}$	$1\times 10^{-4}$
Efficiency(%)	5.73	9.22	10.6	11.21

As evident from Figure 4.3(a) and (b) that the  $J$ - $V$  characteristics is much more sensitive to hole transport than electron transport [38]. The efficiency is reduced drastically if the  $\mu_h\tau'_h$  is less than  $10^{-6}$   $\text{cm}^2/\text{V}$ . It increases slightly with increasing  $\mu_h\tau'_h$  above  $10^{-5}$   $\text{cm}^2/\text{V}$ .



(a)



(b)

**Figure 4.3** Theoretical net current density versus voltage for various levels of  $\mu\tau'$  products of holes and electrons in CdTe Solar cells.

The current-voltage characteristics of a CdTe solar cell as a function CdTe layer thickness is shown in Figure 4.4. All other parameters in figure 4.4 are the same as in figure 4.2. The short circuit current increases with increasing the CdTe layer thickness. However, the charge collection efficiency deteriorates with the CdTe layer thickness and

thus the  $J$ - $V$  curves deviates from the rectangular shape and affects the solar cell efficiency. The solar cell efficiencies are 9.2, 9.7 and 8.9 % for the CdTe thicknesses of 0.5, 1.0 and 2.0  $\mu\text{m}$  respectively.

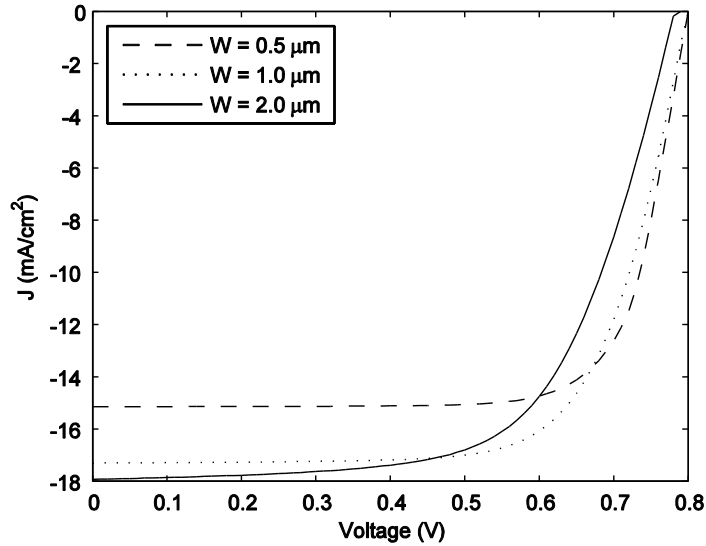


**Figure 4.4** Current-voltage characteristics of a CdTe solar cell as a function CdTe layer thickness.

#### 4.2.1 Effect of CdS window layer on $J$ - $V$ characteristics

As the top window layer is very thin, its effect on  $J$ - $V$  characteristics is ignored in previous models. Its effect is included in the present model (equation 20). The CdS layer thickness may vary from 0.1  $\mu\text{m}$  to 0.3  $\mu\text{m}$  in CdTe solar cells [34]. The effect of CdS layer thickness on the incident sun spectra at CdTe layer is shown in Figure 4.5. Even 0.1  $\mu\text{m}$  thick CdS layer significantly absorbs photons up to 500 nm of wavelength, and thus can reduce the photo current and its overall efficiency. Figure 4.6 shows solar cell efficiency of a CdS/CdTe solar cell as a function of the CdS thickness.

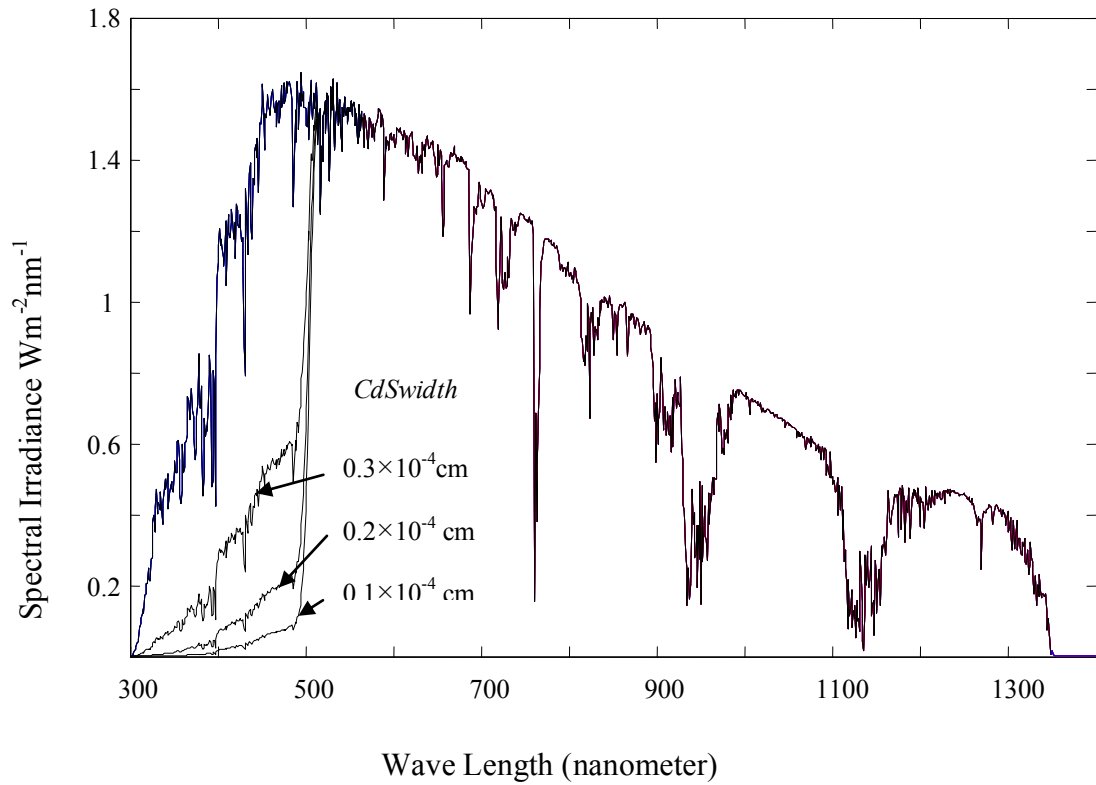


**Figure 4.5** The effect of CdS layer thickness on the incident sun spectra at the CdTe layer. The sun spectra up to 1400 nm is shown since the solar cell is transparent to the photons of wavelengths that are higher than 900 nm.

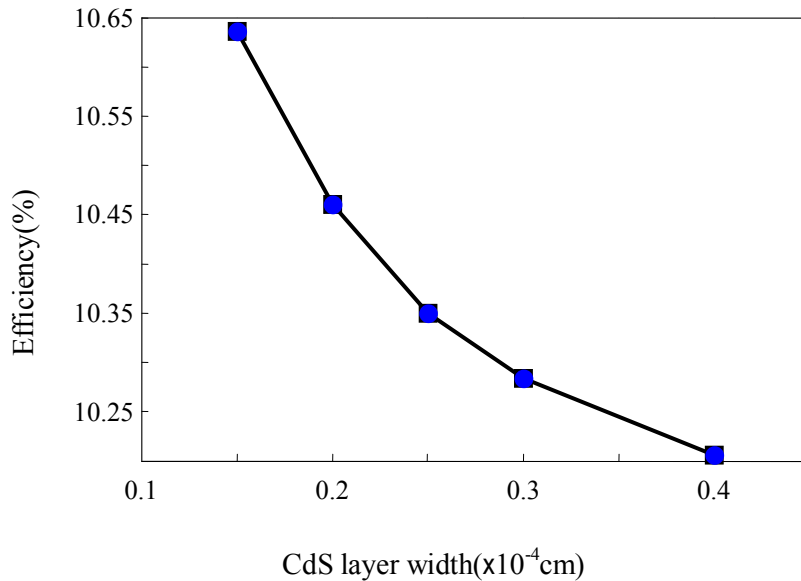


**Figure 4.6** Efficiency vs. thickness of CdS layer graph

#### 4.2.2 Degradation of transport properties of the CdTe and CdS layers

We now validate our model for stressed CdTe solar cell with bilayer back contact. The role of Cu as back contact and the stability during accelerated life testing is an important issue in the study of stressed CdTe solar cell. The performance of CdTe solar cells may degrade over time and the extent of the degradation depends on the absorber and contact materials which is examined by accelerated life testing under stress [39][40][41] and considered as increase in recombination of carriers, resistance, and contact barriers [42]. Cu is used to form cheap and low resistance contact and easy deposition of CdTe but introducing some aspect of degradation [43] [44]. Figure 4.7 shows the  $J-V$  characteristics of a CdTe solar cell with a bilayer back contact of 15 nm Cu/50 nm Ni before and after stress. The CdTe layer thickness is 7  $\mu\text{m}$ . The stressing was done by keeping the cell at 85°C in dry air at 100 % sun illumination at open circuit for

15 days. Assuming typical values for CdTe layer,  $\mu_h = 20 \text{ cm}^2/\text{V}\cdot\text{s}$  and  $\mu_e = 180 \text{ cm}^2/\text{V}\cdot\text{s}$ , the best fit parameters before stress are  $\tau_h = 0.8 \text{ }\mu\text{s}$ ,  $\tau_e = 1 \text{ }\mu\text{s}$ ,  $V_0 = 0.81 \text{ V}$ ,  $A = 1.9$ ,  $R_s = 3.5 \text{ }\Omega\text{-cm}^2$ , and  $R = 0.1$ , whereas after stress the fitted parameters are  $\tau_h = 0.38 \text{ }\mu\text{s}$ ,  $\tau_e = 0.6 \text{ }\mu\text{s}$ ,  $V_0 = 0.77 \text{ V}$ ,  $A = 1.9$ ,  $R_s = 5.2 \text{ }\Omega\text{-cm}^2$ , and  $R = 0.1$ . The overall efficiency varies from 13.4 % to 10.6 % owing to this long time stress. The carrier lifetimes and series resistance deteriorate because of long term stress, which indicates that the transport properties of the CdTe and CdS layers degrade slightly due to stress.

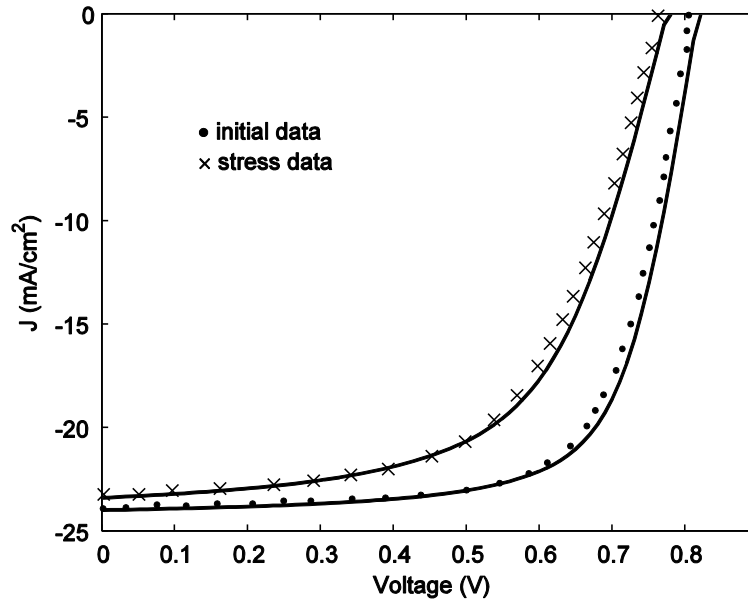


**Figure 4.7** Current-voltage characteristics of a CdTe solar cell before and after stress. The symbols represent experimental data and the solid lines represent the theoretical fit to the experimental data. The experimental data were extracted from Ref [17].

### 4.3 CIGS solar cells

Substrate device structured CIGS solar cell is composed of glass/Mo/Cu(InGa)Se<sub>2</sub>/CdS/ZnO/grid. The Cu(InGa)Se<sub>2</sub> layers deposited by elemental thermal evaporation and their bandgap could be varied from 1.0 to 1.7 eV by varying Ga/(In+Ga). We test our

model with GIGS solar cells. The absorption coefficient for CIGS is obtained from the absorption curves in Ref. [45]. The absorption coefficient for CIGS as a function of photon wavelength is shown in figure 4.8. Figure 4.9 shows the  $J$ - $V$  curves of a GIGS solar cell at 100 % sun intensity. The symbols represent experimental data and the solid lines represent the theoretical fit to the experimental data. The experimental data were extracted from Fig.7 of Ref. [26]. The CIGS thickness is 2  $\mu\text{m}$ . The CdS thickness is assumed as 0.1  $\mu\text{m}$ . The theoretical model shows a very good agreement with the experimental data. The best fit parameters are  $\mu_h \tau_h = 4 \times 10^{-6} \text{ cm}^2/\text{V}$  and  $\mu_e \tau_e = 5 \times 10^{-6} \text{ cm}^2/\text{V}$ ,  $V_0 = 0.64 \text{ V}$ ,  $A = 1.53$ ,  $R_s = 1 \Omega\text{-cm}^2$ , and  $R = 0.23$ . The overall efficiency is 15.5 %. The short circuit current density is 31.8  $\text{mA}/\text{cm}^2$  and the shape of the  $J$ - $V$  curve is almost rectangular, which indicates that the carrier transport properties in CIGS are very good. The CIGS material can efficiently absorb the incident photons up to 1200 nm of wavelength, which gives high short circuit current and high overall efficiency.

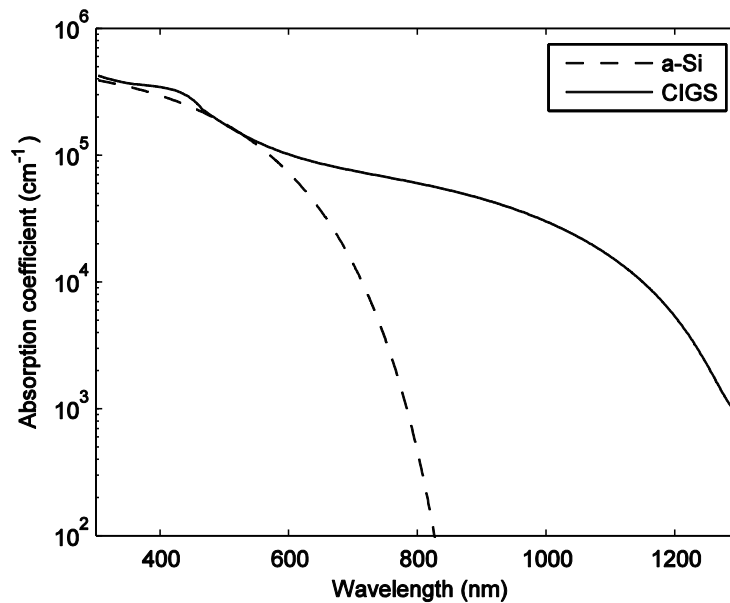


**Figure 4.8** Absorption coefficients of CIGS and a-Si.

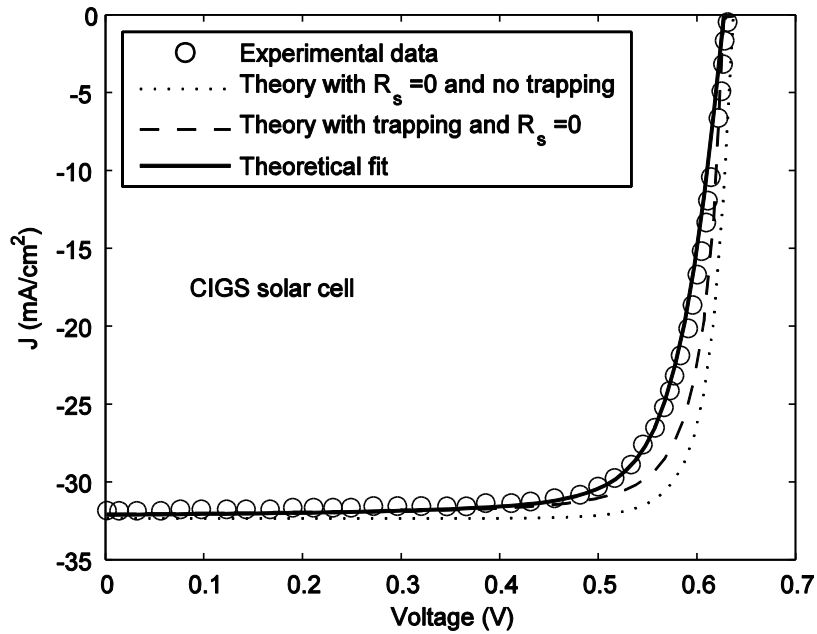


**Figure 4.9** Current-voltage characteristics of a CIGS solar cell. The symbols represent experimental data and the solid lines represent the theoretical fit to the experimental data. The experimental data were extracted from Ref [26].

#### 4.4 Amorphous Si solar cells

The model can also be applied to a-Si:H *p-i-n* solar cells. The absorption coefficient for amorphous silicon is obtained from the absorption curves in Ref. [19], which is plotted in figure 4.8. Figure 4.10 shows the *J-V* curves of an a-Si solar cell at 1 sun intensity. The symbols represent experimental data and the solid lines represent the theoretical fit to the experimental data. The experimental data were extracted from Fig.1 of Ref. [46]. The *i*-layer thickness is 2  $\mu\text{m}$ . The theoretical model shows a very good agreement with the experimental data. The best fit  $\mu\tau'$  of holes and electrons are  $\mu_h\tau'_h = 0.6 \times 10^{-8} \text{ cm}^2/\text{V}$  and  $\mu_e\tau'_e = 1.5 \times 10^{-6} \text{ cm}^2/\text{V}$ , which are consistent with the  $\mu\tau'$  values in a-Si:H [47][48]. The other fitted parameters in Fig. 4.10 are  $V_0 = 0.85 \text{ V}$ ,  $A = 1.6$ ,  $R_s =$

$5\Omega\text{-cm}^2$ , and  $R = 0.1$ . The overall efficiency is 10.2 %. The short circuit current is 17.6  $\text{mA/cm}^2$ . The shape of the  $J/V$  curve indicates that the  $J/V$  characteristics significantly depend on the carrier transport properties in the  $i$ -layer. The a-Si:H material can efficiently absorb the incident photons up to 820 nm of wavelength.

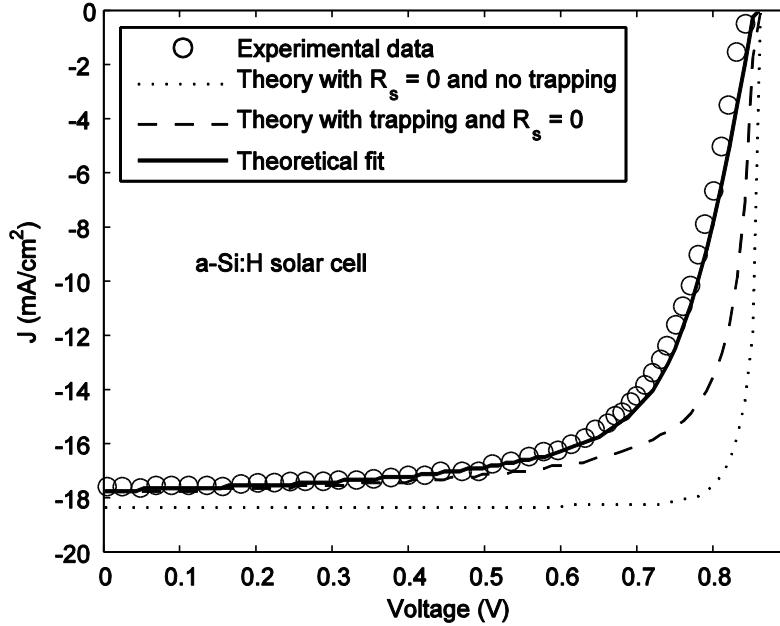


**Figure 4.10** Current-voltage characteristics of an a-Si:H solar cell. The symbols represent experimental data and the solid lines represent the theoretical fit to the experimental data. The experimental data were extracted from Ref [46].

## 4.5 Summary

In this chapter, we analyze the  $J-V$  characteristics of various thin film solar cells with varying carrier transport properties and operating conditions. We validate the proposed model with published experimental data on various thin film solar cells. Actual solar spectrum is used in the calculation which is more close to the physical process that occurs in the solar cell. The recombination current in the depletion region dominates over the

ideal diode current in CdTe solar cells. The solar cell efficiency depends critically on the transport properties of the carriers that drift towards the back contact. The photon absorption capability over a wide spectrum and good carrier transport properties of the absorber layer are equally important for achieving higher efficiency. The analytical model shows a very good agreement with the published experimental data on various thin film solar cells.

# CHAPTER 5 CONCLUSION, CONTRIBUTIONS AND FUTURE WORK

## 5.1 Conclusion

The current-voltage characteristic curve is a useful tool for evaluating the overall performance of a solar cell from where we can determine the efficiency, fill-factor, and maximum output power. We proposed a model in this thesis that describes the  $J/V$  curve of thin film solar cell. The main challenge to model the characteristic of a device is its simplicity and accuracy. Our model is simple and at the same time, it can fit the  $J/V$  characteristic data for different thin film solar cells at different situations like normal condition and stressed condition. We present a closed form expression for  $J/V$  characteristic. In this paper, we solve the continuity equation for both electrons and holes considering exponential photon absorption, exponential electron-hole pair generation across CdTe layer, carrier trapping and carrier drifting in the nearly intrinsic absorber layer. We obtain an analytical expression for the external voltage dependent photo current. The overall load current is calculated considering the effect of voltage dependent forward dark current and the actual solar spectrum. The present model only uses carrier ranges and series resistance as fitting parameters and thus eliminates other fitting parameters such as reverse saturation current and effective attenuation coefficient.

The recombination current in the depletion region dominates over the ideal diode current in CdTe solar cells. The solar cell efficiency depends critically on the transport

properties of the carriers that drift towards the back contact. The photon absorption capability over a wide spectrum and good carrier transport properties of the absorber layer are equally important for achieving higher efficiency. The front window layer has an effect on cell performance, which is first shown in this thesis. The analytical model shows a very good agreement with the published experimental data on various thin film solar cells. The fitting of the model with the published experimental data considering the actual solar spectrum estimates the amount of reflection and other losses in CdTe solar cells.

## **5.2 Contributions**

The contributions of this thesis work are as follows:

- An analytical model is developed to study the current-voltage characteristics of CdS/CdTe thin film solar cells by incorporating exponential photon absorption, carrier trapping and carrier drift in the CdTe layer.
- The overall load current is calculated considering the effect of voltage dependent forward dark current and the actual solar spectrum.
- An analytical expression is derived for the external voltage  $V$  dependent photocurrent.
- The present model only uses carrier ranges and series resistance as fitting parameters and thus eliminates other fitting parameters such as reverse saturation current and effective attenuation coefficient.

- Model validation has been shown by comparing the theoretical results with the recent published experimental results for polycrystalline  $\text{CuIn}_{1-x}\text{Ga}_x\text{Se}$  (CIGS) and hydrogenated amorphous Si (a-Si:H) based solar cells.

### **5.3 Suggestions for Future Work**

The proposed analytical model can be verified by developing a numerical model incorporating detail space charge effects. We have developed our model for CdS/CdTe solar cells and tested the model for CIGS and a-Si. There are other photo sensitive materials available which have a good prospect to use as cell material. Active research is going on with these photoconductive materials so that they could be used to make solar cell viably. By changing the parameters in our model according to the new photoconductive material, the same model can be used to obtain the  $J/V$  characteristic for the corresponding solar cell. The proposed model can also be extended for appropriate application to other *pin/nip* structured cell made of different materials such as organic and nano structured solar cells.

## References

- [1] BP Statistical Review of World Energy June 2009,  
<http://www.bp.com/statisticalreview>
- [2] Rozenzweig et al., Assessment of observed changes and responses in natural and managed systems: Climate Change 2007, (Cambridge University Press, Cambridge, U.K., 2007), pp. 79–131.
- [3] Eray S. Aydil, “Nanomaterials for Solar Cells”, NANOTECHNOLOGY LAW & BUSINESS , Volume 4 No. 3 page 275-291, 2007.
- [4] L. Kazmerski, “Photovoltaics: a review of cell and module technologies”, Renewable and Sustainable Energy Reviews 1, 71-170, 1997.
- [5] Solarbuzz- Solar Market research and analysis, <http://www.solarbuzz.com/facts-and-figures/markets-growth/market-growth>
- [6] [http://www.worldofphotovoltaics.com/financeandmarkets/solar\\_cell\\_production\\_climbs\\_to\\_another\\_record\\_in\\_2009.html](http://www.worldofphotovoltaics.com/financeandmarkets/solar_cell_production_climbs_to_another_record_in_2009.html)
- [7] M. A. Green, K. Emery, Y. Hishikawa, and W. Warta, “Solar cell efficiency table (version 35), Prog. Photovolt: Res. Appl., **18**, 144, 2010.
- [8] S.M. Sze, “Physics of Semiconductor Devices”, 2nd ed., (Wiley, New York, 1981)
- [9] A Rothwarf, J Phillips, N Wyeth, “Junction field and recombination phenomena in the CdS/Cu<sub>2</sub>S solar cell: theory and experiment”, Proceedings of 13th IEEE Photovoltaic Specialists Conference, 399, 1978.
- [10] K Mitchell, A Fahrenbruch, R Bube, “Evaluation of the CdS/CdTe heterojunction solar cell”, Journal of Applied Physics, 48, 4365, 1977.
- [11] R Sudharsanan, A Rohatgi, “Growth and process optimization of CdTe and CdZnTe polycrystalline films for high efficiency solar cells”, Solar Cells, 31, 243, 1991.
- [12] D Fardig, J Phillips, “Characterization of CdTe/CdS solar cells”, Proceedings of 22nd IEEE Photovoltaic Specialists Conference, 1146, 1991.

- [13] M Eron, A Rothwarf, “Effects of a voltage-dependent light-generated current on solar cell measurements: CuInSe<sub>2</sub>/Cd(Zn)S”, Applied Physics Letters, 44, 131, 1984.
- [14] J Phillips, J Titus, D Hoffman, “Determining the voltage dependence of the light generated current in CuInSe<sub>2</sub>-based solar cells using I-V measurements made at different light intensities”, Proceedings of 26th IEEE Photovoltaic Specialists Conference, 463, 1997.
- [15] X. Liu, J.Sites, “Solar-cell collection efficiency and its variation with voltage”, Journal of Applied Physics, 75, 577, 1994.
- [16] S.Hegedus, “Current-voltage analysis of a-Si and a-SiGe solar cells including voltage-dependent photocurrent collection”, Progress in Photovoltaics, 5, 151, 1997.
- [17] Steven Hegedus, Darshini Desai and Chris Thompson, “Voltage dependent photocurrent collection in CdTe/CdS solar cells”, Prog.Photovolt: Res. Appl., 15, pp. 587-602, 2007 and references therein.
- [18] H.G. Wagemann, H. Eschrich, “Grundlagen der PhotovoltaischenEnergiewandlung” (Teubner, Stuttgart 1994) p. 112
- [19] S.M. Sze, “Physics of Semiconductor Devices”, 2nd ed., (Wiley, New York, 1981).
- [20] NREL (<http://trredc.nrel.gov/solar/spectra/am1.5/ASTMG173/ASTMG173.html>)
- [21] T.Komaruet.al, “Improved p-i-n solar cells structure for narrow bandgap a-Si:H prepared by Ar\* chemical annealing at high temperatures”, Solar Energy Materials & Solar Cells 66, 329-335, 2001.
- [22] <http://www.solarserver.com/knowledge/basic-knowledge/photovoltaics.html> (May 2011)
- [23] S. O. Kasap, “Principles of electronic materials and devices,” 2<sup>nd</sup> edition (McGraw-Hill, New York, 2002), chapter 1.

- [24] K. Taretto, U. Rau, J.H. Werner, “Closed-form expression for the current/voltage characteristics of pin solar cells”, Appl. Phys.A 77, 865–871, 2003.
- [25] J. Nelson, “The physics of solar cells”, (Imperial College Press, 2003), chapter 8.
- [26] S. S. Hegedus and W. N. Shafarman, “Thin-film solar cells: device measurements and analysis”, Prog. Photovolt: Res. Appl., 12, pp. 155-176, 2004.
- [27] R Sudharsanan, A Rohatgi, “Growth and process optimization of CdTe and CdZnTe polycrystalline films for high efficiency solar cells”, Solar Cells, 31, 243,1991.
- [28] R.Crandall, “Modeling of thin film solar cells: uniform field approximation”, Journal of Applied Physics, 54, 7176, 1983.
- [29] K Misiakos, F Lindholm, “Analytical and numerical modeling of amorphous silicon *p-i-n* solar cells”, Journal of Applied Physics, 64, 383, 1988.
- [30] **M. S. Anjan** and M. Z. Kabir, “Modeling of current-voltage characteristics of CdS/CdTe solar cells,” Physica Status Solidi A, in press (accepted on May 9, 2011).
- [31] W.Shockley, “Currents to conductors induced by a moving point charge”, J Appl Phys, 9, 635-636, 1938.
- [32] AE Iverson, DL Smith, “Mathematical modeling of photoconductor transient response”, IEEE Trans. Electron Devices, ED-34, 2098-2107, 1987.
- [33] C.-T. Sah, R. N. Noyce and W. Shockley, Proc. Inst. Radio Engrs. 45, 1228 (1957).
- [34] J. Poortmans and V. Arkhipov (eds.), Thin film Solar Cells: Fabrication, Characterization and applications (Wiley & Sons, England, 2006), Chapter 7.
- [35] M. Miyake, K. Murase, T. Hirato, Y. Awakura, “Hall effect measurements on CdTe layers electrodeposited from acidic aqueous electrolyte” J. ElectroanalyticalChem, 562, 247, 2004.

- [36] W.K. Metzger, D. Albin, D. Levi, P. Sheldon, X. Li, B. M. Keyes, and R. K. Ahrenkiel, "Time-resolved photoluminescence studies of CdTe solar cells" *J. Appl. Phys.*, 94, 3549, 2003.
- [37] M. Z. Kabir and S. O. Kasap, "Charge collection and absorption-limited sensitivity of X-ray photoconductors: Applications to a-Se and HgI<sub>2</sub>" *Appl. Phys. Lett.* 80, 1664, 2002.
- [38] **M. S. Anjan** and M. Z. Kabir, "Modeling of current-voltage characteristics of CdS/CdTe solar cells," 4<sup>th</sup> International Conference on Optical, Optoelectronic and Photonic Materials and Applications (ICOOPMA 2010), Budapest, Hungary, August 2010.
- [39] J Hiltner, J Sites. "Stability of CdTe solar cells at elevated temperatures: bias, temperature, and Cu dependence", *Proceedings of 15th NCPV Program Review*, American Institute of Physics, 462, 170,1998.
- [40] S Hegedus, B Mc Candless, R Birkmire. "Analysis of stress-induced degradation in CdS/CdTe solar cells", *Proceedings of 28th IEEE Photovoltaic Specialists Conference*, 535, 2000.
- [41] D Albin, D Levi, S Asher, A Balcioglu, R Dhere. "Precontact surface chemistry effects on CdS/CdTe solar cell performance and stability", *Proceedings of 28th IEEE Photovoltaic Specialists Conference*, 583, 2000.
- [42] S Hegedus, B McCandless. "CdTe contacts for CdTe/CdS solar cells: effect of Cu thickness, surface preparation and recontacting on device performance and stability", *Solar Energy Materials and Solar Cells*, 88, 75, 2005.
- [43] C Corwine, A Pudov, M Gloeckler, S Demtsu, J Sites. "Copper inclusion and migration from the back contact in CdTe solar cells", *Solar Energy Materials and Solar Cells*, 82, 481, 2004.

- [44] D. Grecu, A. Compaan, D. Young, U. Jayamaha, D. Rose. “Photoluminescence of Cu-doped CdTe and related stability issues in CdS/CdTe solar cells”. Applied Physics Letters, 88, 2490, 2000.
- [45] S.-H. Hana and A. M. Hermann, Effect of Cu deficiency on the optical properties and electronic structure of CuInSe<sub>2</sub> and CuIn<sub>0.8</sub>Ga<sub>0.2</sub>Se<sub>2</sub> determined by spectroscopic ellipsometry, Appl. Phys. Letts., 85, 576-578, 2004.
- [46] E. Klimovsky, J.K. Rath, R.E.I. Schropp, F.A. Rubinelli, “Modeling a-Si:H *p-i-n* solar cells with the defect pool model”, J. non-crystalline Solids, 338–340, 686–689, 2004.
- [47] R. A. Street (Ed.), Technology and applications of Amorphous Silicon (Springer-Verlag 2000), page 151.
- [48] W. B. Jackson, S. M. Kelso, C. C. Tsai, J. W. Allen, and S. -J. Oh, “Energy dependence of the optical matrix element in hydrogenated amorphous and crystalline silicon” Phys. Rev. B 31, p-5187, 1985.